https://ntrs.nasa.gov/search.jsp?R=19780007939 2020-03-22T05:31:19+00:00Z

SC5046.25FR

HIGH SENSITIVITY 1.06 μm OPTICAL RECEIVER FOR PRECISION LASER RANGE FINDING

By

Frederick W. Scholl
James S. Harris, Jr.

Rockwell International/Science Center
1049 Camino Dos Rios
Thousand Oaks, California 91360

Prepared Under Contract No. NAS5-22806

January 1977

FINAL REPORT for period October 1, 1975 thru September 30, 1976

Prepared for:

National Aeronautics & Space Administration
Goddard Space Flight Center
Greenbelt Road
Greenbelt, MD 20771

Approved for public release; distribution unlimited

UNCLASSIFIED

SECURITY CLASSIFICATION OF THIS PAGE (When Data Entered)

REPORT DOCUMENTATION PAGE

READ INSTRUCTIONS BEFORE COMPLETING FORM

1. REPORT NUMBER	2. GOVT ACCESSION NO.	3. RECIPIENT'S CATALOG NUMBER
4. TITLE (and Subtitle) High Sensitivity 1.06μm Optical Receiver for Precision Laser Range Finding		5. TYPE OF REPORT & PERIOD COVERED Final Report, Type III 10/01/75 thru 09/30/76
		6. PERFORMING ORG. REPORT NUMBER SC5046.25FR
7. AUTHOR(s) Frederick W. Scholl, James S. Harris, Jr.		8. CONTRACT OR GRANT NUMBER(s) NAS5-22806
9. PERFORMING ORGANIZATION NAME AND ADDRESS Rockwell International/Science Center, 1049 Camino Dos Rios, Thousand Oaks, CA 91360		10. PROGRAM ELEMENT, PROJECT, TASK AREA & WORK UNIT NUMBERS
11. CONTROLLING OFFICE NAME AND ADDRESS National Aeronautics & Space Administration, Goddard Space Flight Center, Greenbelt Rd., Greenbelt, MD 20771		12. REPORT DATE January 1977
		13. NUMBER OF PAGES 53
14. MONITORING AGENCY NAME & ADDRESS(if different from Controlling Office)		15. SECURITY CLASS. (of this report) Unclassified
		15a. DECLASSIFICATION/DOWNGRADING SCHEDULE

16. DISTRIBUTION STATEMENT (of this Report)

Approved for public release; distribution unlimited

17. DISTRIBUTION STATEMENT (of the abstract entered in Block 20, if different from Report)

18. SUPPLEMENTARY NOTES

19. KEY WORDS (Continue on reverse side if necessary and identify by block number)

1.06μm Nd:YAG Laser
Laser Rangefinding
Avalanche Photodiode
AlGaSb Epitaxy
Liquid Phase Epitaxy

20. ABSTRACT (Continue on reverse side if necessary and identify by block number)

In this report the design, fabrication, and evaluation of 1.06μm AlGaSb avalanche photodiodes is reported. The photodectors are designed for use in a low noise optical receiver suitable for 2 cm accuracy rangefinding with 10-100 received 1.064μm photons. Work described in this report emphasized (1) design of suitable photodetector structures, (2) epitaxial growth of AlGaSb devices, (3) fabrication of photodectors, and (4) electro-optics characterization. AlGaSb APDs with average gain of 10, internal quantum

DD FORM 1 JAN 73 1473 EDITION OF 1 NOV 65 IS OBSOLETE

UNCLASSIFIED

SECURITY CLASSIFICATION OF THIS PAGE (When Data Entered)

efficiency of > 60%, capacitance less than 0.2 pf, and dark current of less than 1μa were produced.

Rockwell International
Science Center

TABLE OF CONTENTS

		Page
1.0	INTRODUCTION AND SUMMARY	1-1
2.0	PROGRAM GOALS AND APPROACH	2-1
	2.1 Systems Performance	2-1
	2.2 Materials	2-5
	2.3 Device Design	2-7
3.0	RESULTS	3-1
	3.1 Avalanche Photodiode Performance and Characterization	3-1
	3.2 Materials Growth and Evaluation	3-5
	3.3 Device Processing	3-20
	3.4 Device Performance	3-22
4.0	CONCLUSIONS AND RECOMMENDATIONS	4-1
5.0	REFERENCES	5-1

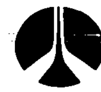

LIST OF ILLUSTRATIONS

		Page
Fig. 2.1	Bandgap-lattice constant diagram for alloys of III-V semiconductors	2-6
Fig. 2.2	AlGaSb band structure	2-8
Fig. 2.3	AlGaSb APD structure. Enough Al is added to top window layer to attain virtual 100% quantum efficiency	2-9
Fig. 3.1	Avalanche gain characteristics	3-3
Fig. 3.2	Effect of gain non-uniformities on excess noise	3-6
Fig. 3.3	AlGaSb liquidus isotherms. Experimental data points at 500°C and calculated fit using the values of Table 1	3-8
Fig. 3.4	$Al_xGa_{(1-x)}Sb$ solidus isotherms. Experimental data points at 500°C and computer fit using the values of Table 1	3-9
Fig. 3.5	Four layer $Al_xGa_{1-x}Sb$ APD structure. Note excellent growth morphology	3-10
Fig. 3.6	Cleaved cross-section (stained) of four layer 1.06μm $Al_xGa_{1-x}Sb$ APD. Layers grown on n^+ GaSb substrate are: n $Al_{.115}Ga_{.885}Sb/n^-Al_{.23}Ga_{.77}Sb/p^+ Al_{.23}Ga_{.77}Sb/p^+ Al_{.4}Ga_{.6}Sb$	3-11
Fig. 3.7	Surface topology of GaAlSb and GaAsSb	3-12
Fig. 3.8	n, Te doped $Ga_{.77}Al_{.23}Sb$	3-14
Fig. 3.9	Effect of doping variations on gain. $\lambda = \alpha/\beta$. p^+/n^- junction	3-15

LIST OF ILLUSTRATIONS (Cont'd)

Page

Fig. 3.10 Heterojunction device structure for optical transmission measurements. The photocurrent measured in the GaSb p-n junction is due solely to light transmitted through the top $Ga_{1-x}Al_xSb$ layer . . . 3-17

Fig. 3.11 p-n junction structure for optical transmission measurement . . . 3-18

Fig. 3.12 Etched mesa--3 mil x 3 mil--with 1 mil metalization pad . . . 3-20

Fig. 3.13 $Al_xGa_{1-x}Sb$ APD structure . . . 3-22

Fig. 3.14 C-V for 3 mil x 3 mil AlGaSb APD . . . 3-23

Fig. 3.15 Photoresponse of 3 layer AlGaSb APD . . . 3-25

Fig. 3.16 Photoresponse of 4 layer AlGaSb APD . . . 3-26

Fig. 3.17 Reverse bias I-V characteristic and photocurrent gain for a 1.064μm $Al_{.23}Ga_{.77}Sb$ avalanche photodiode . . . 3-27

Fig. 3.18 High breakdown AlGaSb photodiode; growth F10-9/23/76 . . . 3-28

Fig. 3.19 APD pulse response. Diode from growth F9-4/23/76 . . . 3-29

Fig. 3.20 Linear scans showing gain in 3 mil diam mesa devices from growth F10-5/24/76, (a) $\overline{M}$ = 8.5, (b) $\overline{M}$ = 12 . . . 3-31

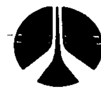

LIST OF ILLUSTRATIONS (Cont'd)

Page

Fig. 3.21 Gain profiles from growth F10-8/21/76. 3 mil x 3 mil square mesa devices. (a) $\overline{M}$ = 10, (b) $\overline{M}$ = 17.5 3-32

1.0 INTRODUCTION AND SUMMARY

This report describes progress toward realization of a high sensitivity optical receiver for precision rangefinding at 1.064μm. Overall objective is 2 cm accuracy with 10-100 received photons. These requirements are based on current NASA efforts to develop a spaceborne rangefinder for geodetic surveying. Evaluation of existing detector technologies -- Si APD's and alloy photocathodes -- indicated that a new receiver approach is required in order to meet these goals. A III-V alloy 1.06μm avalanche photodiode receiver has been chosen as the most promising candidate. Principal efforts in the present contract were focused on improving the performance of the 1.06μm avalanche photodiode, this device being the key element in the receiver. These efforts resulted in AlGaSb avalanche photodiodes with average gains of 10, dark currents of <1μa and capacitance <0.2 pf. These photodiodes represent a significant achievement in the 1.06μm receiver technology development program. Under previous contract work with NASA and Air Force support (Air Force Contract F33615-74-C-1030, NASA Contracts NAS5-23333 and NAS5-23134) we have successfully demonstrated the 1.06μm receiver concept by design and fabrication of hybrid integrated GaAs FET transimpedence amplifier receivers. These APD receivers showed 95% quantum efficiency at 1.06μm with pulse sensitivity of 379 photons (peak output voltage = rms noise output voltage) and 10-90% risetimes of 250 ps. They demonstrated that the rangefinder goals could be met if photodiodes of sufficient avalanche gain (>20) could be produced. This was the principal thrust behind the work we report here.

The key factor in avalanche photodiode development is material quality; thus most of the program effort was devoted to material development and characterization. AlGaSb alloys were of greatest interest. Improvements in average avalanche gain and gain uniformity were sought and, to a significant extent, attained. Suitable epitaxial growth procedures were developed for fabrication of high quantum efficiency, low capacitance hterojunction device designs. Device processing and packaging techniques were designed and, to date, partially implemented.

The APDs developed during the past year provide a strong foundation from which further development may fruitfully grow. Improvements in average gain and gain uniformity are probably desirable. Measurements of excess multiplication noise need to be carried out. These measurements along with suitable systems modelling will be essential in predicting the expected range accuracy.

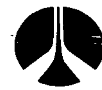

2.0 PROGRAM GOALS AND APPROACH

The overall objective of this program is the development of a 1.06μm optical receiver suitable for precision rangefinding with 2 cm accuracy and 10-100 received photons. The immediate objective of the work reported here was the development of an avalanche photodiode with which such a receiver could be implemented. Design goals for the APD may be summarized: QE $\geq$ 95%; 50Ω impulse response (FWHM) = 100 ps; average avalanche gain = 30 (±10% uniformity). Stability of these parameters with time is obviously assumed. The APD requirements are determined by the details of the pulse signal-to-noise ratio. These are discussed in Section 2.1. Material and device design approaches are then described in Sections 2.2 and 2.3.

2.1 *Systems Performance*

The overall objective of this program is to develop an avalanche photodiode receiver for 1.06μm rangefinding. However, at the present time, very little, if any, practical experience with such a system is available. The key question is: "What is the range accuracy that can be achieved with the avalanche photodiode receiver?" For nearly ideal amplifiers such as the PMT, range accuracy will be shot noise limited; this is, of course, the ultimate performance limit. Avalanche photodetectors, on the other hand, suffer from excess noise and time jitter, both intrinsic to the two-carrier gain process itself. These effects are expected to degrade the ultimate range accuracy to somewhat less than the shot noise limit. In addition, the usual thermal noise contribution to range error must be considered. Complete theoretical evaluation of all these noise sources is currently in a preliminary state. Here we give a simplified discussion of range accuracy; considering first thermal and secondly quantum noise limitations.

Let us consider an optical receiver with an incident number of photons, N_{ph}, in a light pulse on the detector. If the quantum efficiency is η and the average avalanche gain is M, then the number of electrons flowing in the preamp input is

$$N_e = \eta \, M \, N_{ph} \tag{2.1}$$

and the total charge is

$$Q_p = q \eta M N_{ph}. \qquad (2.2)$$

In general, such a charge pulse will produce an output voltage pulse from the preamplifier, the peak value of which, V_p will be proportional to Q_p, i.e.,

$$V_p = \left(\frac{V}{Q}\right)_p Q_p \qquad (2.3)$$

The constant of proportionality or "pulse gain", $(V/Q)_p$ will depend on the bandwidth characteristics of the receiver and the shape of the incident pulse. In the limit of an infinitely short (δ-function) incident current pulse into the preamp, there is a characteristic output pulse waveform $V_\delta(t)$ and pulse gain $(V/Q)_\delta$ which depend only on the preamplifier gain characteristics. The response $V(t)$ to any arbitrary input current pulse, $i(t)$ can be obtained from $V_\delta(t)$ by convolving $i(t)$ with $V_\delta(t)$.

In addition to the signal output pulse, the preamplifier also exhibits some rms noise output voltage, v_{no}. If there were no output voltage noise then the receiver would give virtually unlimited time resolution when followed by a constant-fraction discriminator (CFD) (limited only by jitter in the CFD and time jitter in the detector itself - which is extremely small in the $GaAs_{1-x}Sb_x$ APD). If we are trying to measure a time t_o at which (without noise) $V(t)$ would cross some level V_o, then the effect of noise is to introduce an uncertainty in $V(t)$ which at all times is given by some probability function. If we assume that the slope of $V(t)$, $\frac{dV}{dt}$, is essentially constant over the region $V_o \pm v_{no}$ or $V_o \pm 2\, v_{no}$, then the time uncertainty in when $V(t)$ will actually cross V_o is given by the same shaped probability function as the voltage noise, only with the voltage horizontal scale replaced by voltage divided by dV/dt. Hence the rms time uncertainty, ΔT_{rms}, in $V(t)$ crossing V_o is given by

$$\Delta T_{rms} = \frac{v_{no}}{\left(\frac{dV}{dt}\right)_{t=t_o}} \qquad (2.4)$$

where v_{no} is the rms output noise.

The slope $(dV/dt)_{t=t_o}$ can be approximated by more commonly measured receiver parameters as

$$(dV/dt)_{t=t_o} = V_p/T_{PR}, \tag{2.5}$$

where T_{PR} is the pulse risetime. Substituting Eq. 2.5 in Eq. 2.4, we have

$$\Delta T_{rms} = \frac{v_{no}}{V_p} T_{PR}, \tag{2.6}$$

where it is assumed that V_p is considerably greater than v_{no} (the false alarm rate would obviously be unacceptably high if it were not, anyway). This expression can further be related to the preamplifier parameters discussed earlier by substituting Eq. 2.3, giving

$$\Delta T_{rms} = \frac{v_{no}}{\left(\frac{V}{Q}\right)_p Q_p} T_{PR} \tag{2.7}$$

or from Eqs. 2.1 and 2.2

$$\Delta T_{rms} = \frac{v_{no}}{q\left(\frac{V}{Q}\right)_p} \frac{T_{PR}}{N_e} \tag{2.8}$$

where $(V/Q)_p$ is the "pulse gain" and N_e the number of electrons flowing in the preamp input. The "minimum detectable current pulse" of the preamp, N_{op} is given by

$$N_{op} = \frac{v_{no}}{q\left(\frac{V}{Q}\right)_p} \tag{2.9}$$

N_{op} is just the number of electrons in a current pulse required to make the peak output voltage equal the rms output noise. In terms of N_{op} then, Eq. 2.8 becomes (assuming N_e considerably greater than N_{op})

$$\Delta T_{rms} = \frac{N_{op}}{N_e} T_{PR} . \tag{2.10}$$

This can be expressed in terms of the number of photons in the light pulse, N_{ph}, the quantum efficiency, η, and average avalanche gain, M from Eq. 2.1 by

$$\Delta T_{rms} = \frac{N_{op} T_{PR}}{\eta M N_{ph}} \tag{2.11}$$

Conversely, the minimum level of avalanche gain required for single pulse detection of N_{ph} photons with rms time resolution ΔT_{rms} is given by

$$M_{MIN} = \frac{N_{op}}{\eta N_{ph}} \frac{T_{PR}}{\Delta T_{rms}} \tag{2.12}$$

(valid for $T_{PR} > 2 \Delta T_{rms}$ or so). M_{MIN} is a lower bound figure ignoring multiplied shot noise which could be dominant for high M's and $T_{PR} >> \Delta T_{rms}$. Note that in general using fast optical pulses with a fast receiver (giving short T_{PR} and lower N_{op}) improves the signal-to-noise ratio and time resolution and reduces the requirement for high avalanche gain.

The measured performance of the GaAsSb 1.06μm receivers developed under NASA Contracts NAS5-23134 and NAS5-23333 and Air Force Contract F33615-74-C-1030 can be used to obtain a numerical estimate of M_{MIN} from Eq. 2.12. For the best hybrid integrated receiver delivered under these programs, $\eta = 0.96$, $N_O = 379$ electrons and $T_{PR} = 250$ ps. For 2 cm accuracy, $\Delta T_{rms} = 133$ ps, and so we find $M_{MIN} = 7.5$ for $N_{ph} = 100$ photons and $M_{MIN} = 75$ for $N_{ph} = 10$ photons. These numbers give an estimate of the required avalanche gain for signal levels of interest in this program.

Avalanche multiplication noise is expected to degrade the range accuracy from the values discussed above. This effect becomes more significant at higher gains (lower signal levels). A crude estimate of range accuracy degradation can be obtained by consideration of high gain shot noise limited operation (neglect thermal noise).

Let the rectangular received pulses have width T and, on the average, N_{ph} photons (N_{ph} = 10-100). Suppose the time discriminator counts photons and extracts range information when $N_{ph}/2$ have been counted. The rms single

shot time uncertainty, for pure Poisson statistics (no avalanche gain) is:

$$\Delta\bar{r}_{rms} = \frac{\sqrt{N_{ph/2}}}{N_{ph}/T} = \frac{T}{\sqrt{2N_{ph}}} \tag{2.13}$$

For a 400 ps wide pulse, 5 photons/pulse should be adequate for 2 cm range accuracy (neglecting other noise sources and assuming unity quantum efficiency). With average avalanchegain M, we find the range accuracy degraded to

$$\Delta t_{rms} = \frac{T}{\sqrt{2N_{ph}}} \; M^{X_N/2} \quad ,$$

where X_N is the excess noise coefficient. For, say, M = 30, and X_N = 0.4 (appropriate actually to silicon APDs), we find $M^{X_N/2} \cong 2$. In other words, the expected limiting range accuracy will be twice as poor as would be expected from signal shot noise alone.

Further systems modelling still remains to be done. Adequate false alarm rates must be established. A more accurate calculation of Poisson limited range accuracy is needed. This will include a realistic model of the discriminator and a more extensive APD model. The latter must include fluctuations in amplitude and time origin of the multiplied charge.

2.2 Materials

The heterojunction III-V alloy materials technology provides the only viable approach to fabricating photodiodes suitable for precision 1.06μm rangefinding. Figure 2.1 shows the bandgap and lattice constant of the principle binary III-V's and their ternary alloys. For operation at 1.064μm (1.17 eV) we require an active absorbing layer with bandgap of ≈ 1.1 eV. Smaller gap results in excess dark current; larger bandgap results in low quantum efficiency. GaInAs, InGaAsP and GaAlSb; of these four only the latter two can be grown on lattice matched substrates (InP and GaSb). At present, the material quality of the quaternary InGaAsP is not established. On the other hand, our previous work on AlGaSb 1.8μm photocathodes (NVL Contract No. DAAK03-73-C-0231)

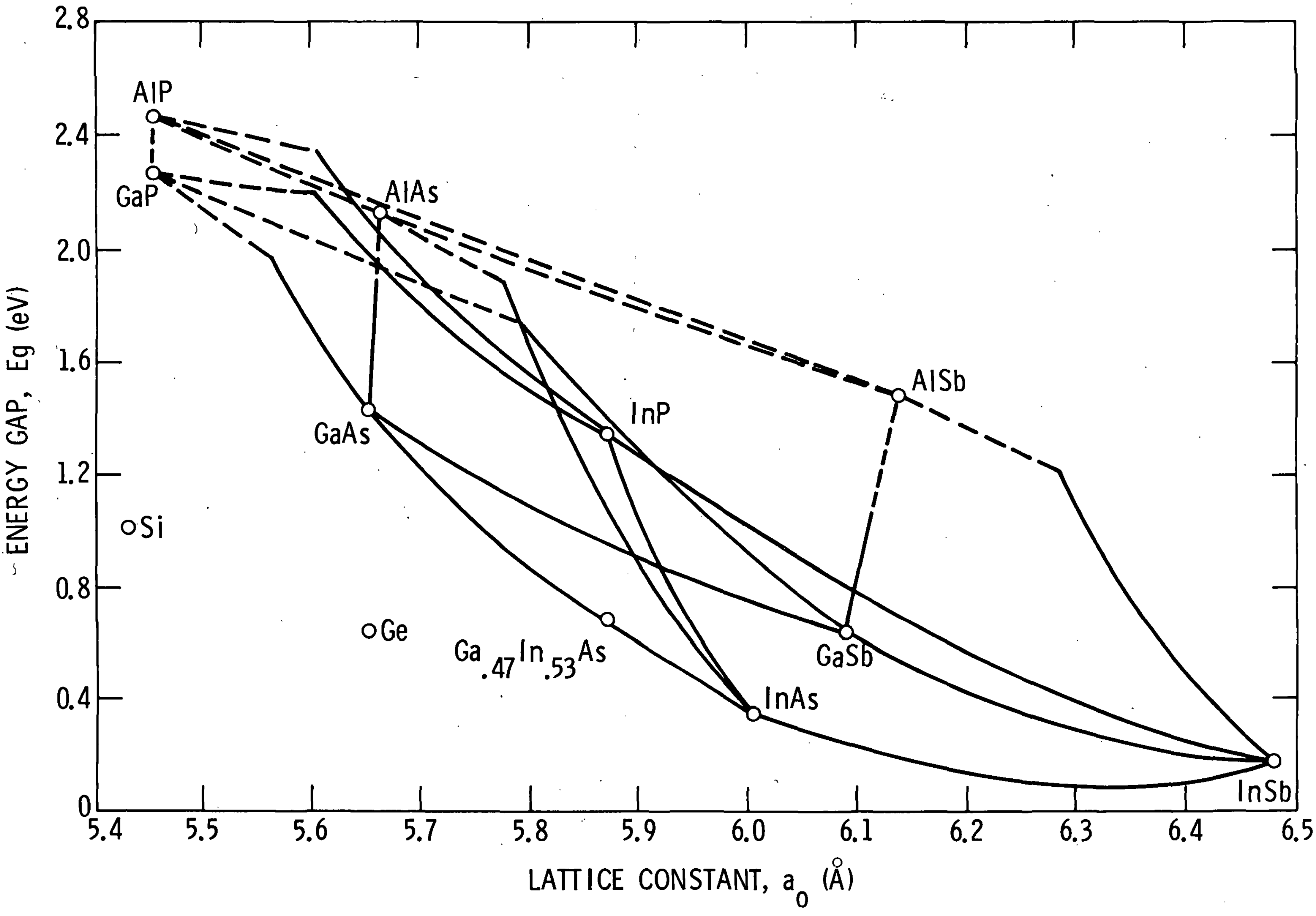

Fig. 2.1 Bandgap-lattice constant diagram for alloys of III-V semiconductors.

had demonstrated that device quality multilayer structures with controlled doping could be fabricated from AlGaSb alloys. Thus we elected to develop this material for 1.06μm avalanche photodiodes.

The experimentally determined AlGaSb band structure over the whole range of compositions is shown in Fig. 2.2.[1] This diagram is relatively well established except at the AlSb end, where the ordering of the X and L minima is still uncertain. For most of the alloy composition range, it is seen that AlGaSb is an <u>indirect</u> semiconductor with L (or X) conduction band minima. Fabrication of high performance heterojunction photodiodes requires two alloy layers: the first, active layer, must strongly absorb (~ 1-2μm absorption depth) at 1.064μm; the second, window layer, must have zero absorption at 1.064μm. Reference to Fig. 2.2 shows that alloys with 23-30% AlSb have suitable direct (Γ) minima for absorber layers, while those with 35-40% AlSb can serve as transparent window layers. The other details of the band structure are largely irrelevant to APD design. The actual separations and orderings of the 3 non-equivalent conduction band minima may well influence the microscopic electron and hole ionization rates, but the band structure obviously cannot be altered to provide more favorable avalanche gain.

2.3 Device Design

A suitable device structure may be based on the materials available. One such design is shown in Fig. 2.3. This structure contains (1) buffer layer of 11.5% AlSb, (2) field termination layer of p^+ $Ga_{77}Al_{23}Sb$, (3) active depleted layer of n^- $Ga_{77}Al_{23}Sb$, (4) window layer, transparent to 1.06μm, of $Ga_{60}Al_{40}Sb$. With suitable antireflection coating on the $Ga_{.6}Al_{.4}Sb$ surface virtually 100% of all incident photons can be rapidly (transit time ~ 5×10^{-4} cm/10^7 cm/s = 50 ps) collected by the n^- layer. This layer is fully depleted at operating bias. The parallel equipotentials and strong optical absorption ensure an rms transit time dispersion of less than $\frac{1}{\sqrt{2\alpha V_s}}$ = 7.07 ps (at unity gain).

The device structure shown in Fig. 2.3 offers virtually 100% quantum efficiency, minimum excess multiplication noise, no diffusion tail or "back porch," and immunity to surface breakdown. At operating bias, as noted above, the n^- layer is fully depleted; thus all incident carriers immediately see the

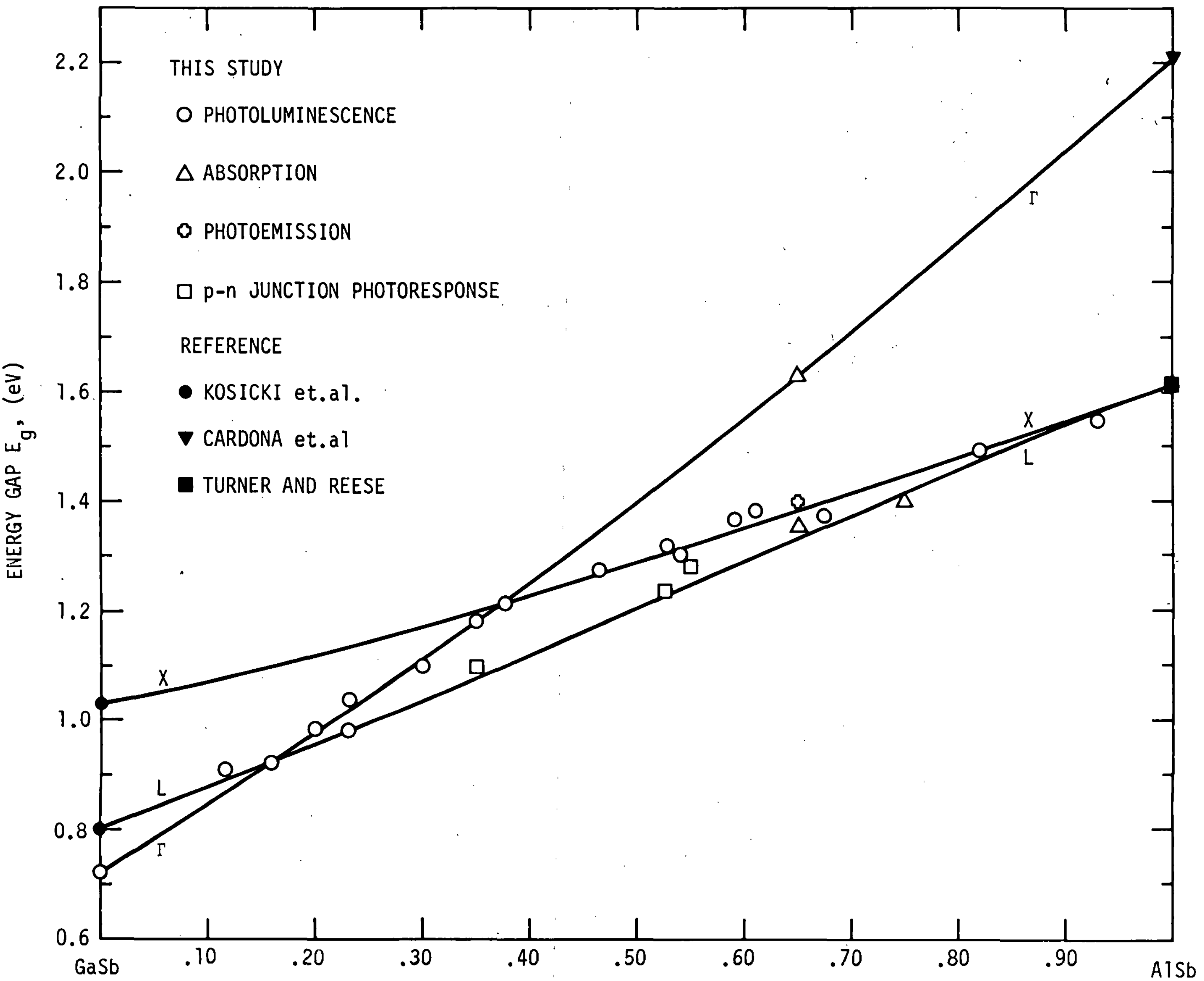

Fig. 2.2 AlGaSb Band Structure.

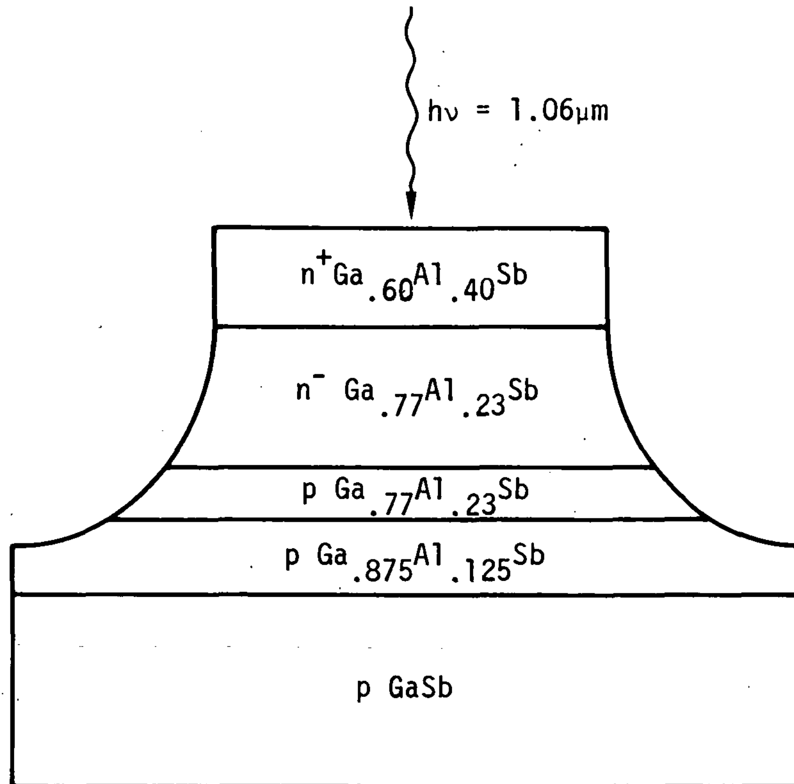

Fig. 2.3 AlGaSb APD Structure. Enough Al is added to top window layer to attain virtual 100% quantum efficiency.

large junction potential. The resultant photocurrent is ideally "pure" in that it consists entirely of holes (in this case). This situation results in the least excess multiplication noise, assuming, of course, that $\beta > \alpha$ (β = hole ionization rate, α = electron ionization rate, both in cm^{-1}). If $\beta < \alpha$, obviously the complementary structure would be grown. The p^+/n^- layer sequence yields a device geometry which should be immune to surface breakdown. Mesa diodes have a cross-section which increases as one moves away from the top surface of the mesa. This geometrical factor, combined with the layer sequence of Fig. 2.3, results in surface electric fields considerably lower than the bulk fields. Thus uniform bulk avalanche results.

3.0 RESULTS

This contract work resulted in the first AlGaSb 1.06μm avalanche photodiodes ever fabricated. Average gains of 10 were observed. The materials work and device fabrication technologies developed to support this are described here. Detailed measurements on the photodiodes are described. Some preliminary background on avalanche photodiode performance and characterization are first given.

3.1 Avalanche Photodiode Performance and Characterization

The key parameters in avalanche photodiode performance are the average multiplication, multiplication areal uniformity and excess multiplication noise. These quantities and suitable theoretical descriptions are reasonably well developed for silicon avalanche detectors[2]. However, for III-V compound and III-V alloy detectors complete descriptions of avalanche performance do not exist; in fact, considerable discrepancies are found in the available literature. Neither is it clear whether the physics of avalanche multiplication is significantly different in polar III-V and elemental semiconductors.

The avalanche gain, M, is simply the ratio of the measured photocurrent at bias V to the primary photocurrent at the same bias

$$I = M(V)I_{primary}(V) \tag{3.1}$$

For experimental purposes the avalanche diodes are designed so that the primary photocurrent is both independent of bias and composed either of holes or electrons but not both; one then measures the fundamental hole and electron multiplications. These two quantities, denoted by M_n and M_p, can always be measured by growing and testing two complementary diodes, i.e., n on p and p on n. In general, one would find $M_n \neq M_p$ and then practical diodes are of course fabricated using the favorable carrier. In some cases, one can arrange to measure M_n and M_p in the <u>same diode</u>. Since E(V) is then known for both measurements, they can then be used determine the microscopic ionization rates α (electrons) and β holes, both expressed in cm^{-1}.

The measured multiplications are expressed in terms of these quantities as follows (W = depletion width):

$$1 - \frac{1}{M_n} = \int_o^W \alpha \, e^{-\int_o^x (\alpha-\beta)dx'} dx$$

$$1 - \frac{1}{M_p} = \int_o^W \beta \, e^{\int_x^W (\alpha-\beta)dx'} dx \qquad (3.2)$$

By assuming the ionization rates are local in character (i.e. dependent on field only), these equations can be inverted to express α and β in terms of the measured M_n and M_p[3,4]. The ionization rate ratio α/β influences considerably the measured photodetector properties. For a diode with constant field depletion region (p-i-n structure) we have

$$M_n = \frac{1}{1 - \alpha W} \quad \text{if } \frac{\beta}{\alpha} = 1$$

$$M_n = e^{\alpha W} \quad \text{if } \frac{\beta}{\alpha} = 0 \qquad (3.3)$$

These two characteristics are plotted in Fig. 3.1.; the advantages of $\beta/\alpha=0$ are obvious. A material with small α/β is clearly desirable for fabrication of large area avalanche diodes. All else being equal, such a material would be preferred over a material with $\beta/\alpha \approx 1$.

The ionization rate ratio also influences the noise performance of the photodiode. Again the case $\beta/\alpha = 0$ is preferred and leads to current amplification with the smallest decrease in signal-to-noise ratio (shot noise

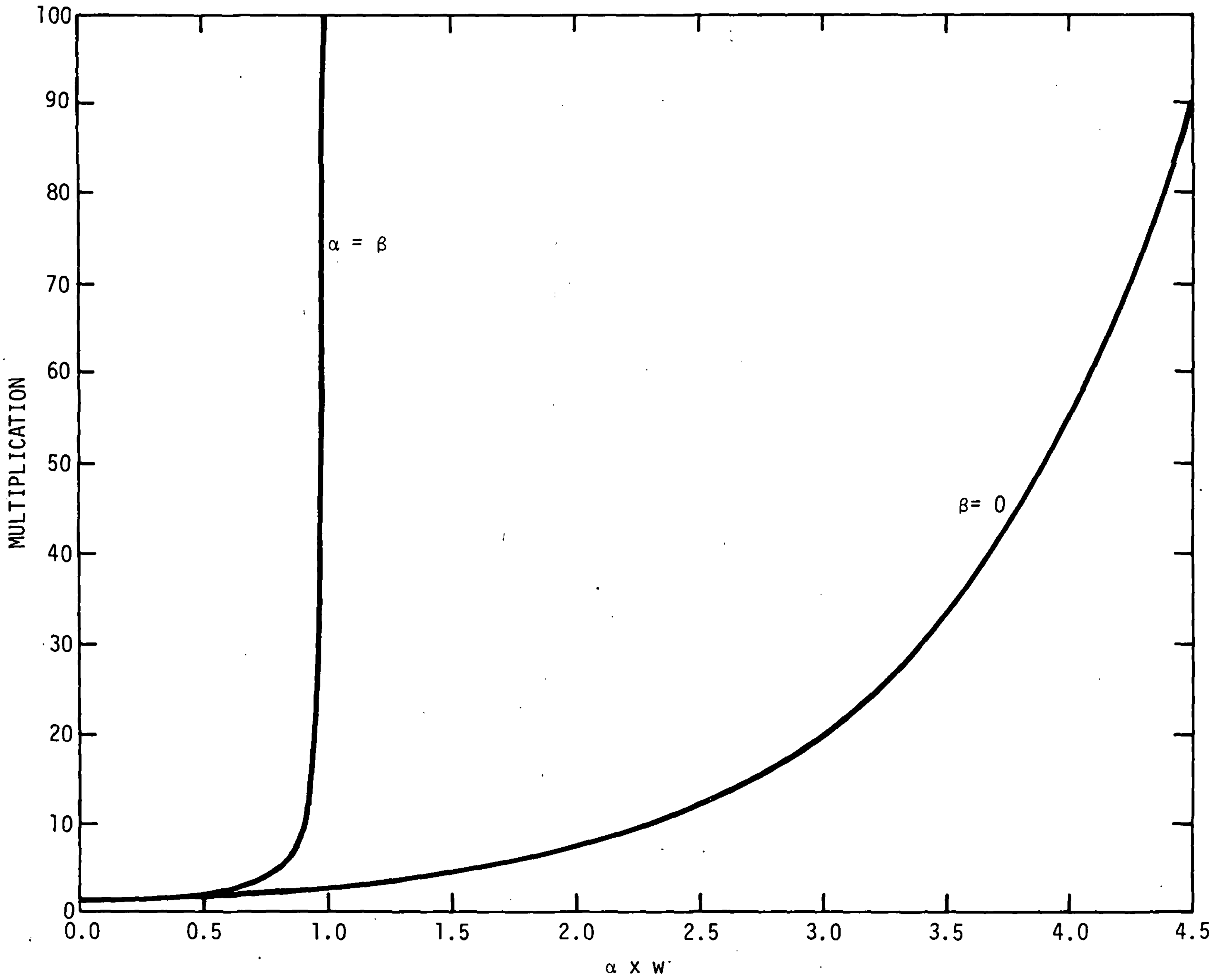

Fig. 3.1 Avalanche gain characteristics.

only). For all cases, the variance of the multiplied signal is increased by the excess noise factor F(M):

$$\langle i^2 \rangle = 2q\eta I_{ph} M^2 F(M) \quad \Delta f, \tag{3.4}$$

where F(M) is given by (electron multiplication)

$$F(M) = \beta/\alpha \ M + (2 - \frac{1}{M}) \ (1 - \beta/\alpha) \tag{3.5}$$

For the ideal case $\beta/\alpha = 0$, we find only a 3dB reduction in signal-to-noise ratio. For the other limiting case, $\beta/\alpha = 1$, the signal-to-noise ratio is decreased by 1/M. These results seem to be verified by experimental work on silicon APDs. However, for III-V detectors (GaAs, InGaAs), the excellent reported noise performance is at variance with the measured ionization rates[5,6,7,8]. Further measurements are required.

Another potentially important source of noise in avalanche detectors are the gain non-uniformities commonly observed in practical devices. Equations 3.4 and 3.5 of course describe the properties of a perfectly uniform diode. For a non-uniform diode, uniformly illuminated over its area A, we have

$$\frac{F}{F_{av}} = \frac{1}{A} \iint \frac{M^2(x,y)}{M_{av}^2} \frac{F(M)}{F_{av}} \ dxdy, \tag{3.6}$$

where M(x,y) is the local gain at point (x,y). F/F_{av} is simply the ratio of the actual excess noise factor to the noise factor for a <u>uniform</u> diode with the same average gain, M_{av}. It thus represents the increase in noise due to gain non-uniformities.

Numerical results were obtained for a simple square photodiode with sinusoidal gain variation:

$$M(x,y) = M_{av} + \Delta M \sin(\frac{2\pi}{a} x) \quad 0<x,y<a$$

The results are shown in Fig. 3.2. With an average gain of 20±50% (gain varying between 30 and 10) we pay a penalty of about 1 dB in increased shot noise. This would probably be acceptable for rangefinder applications.

From this discussion, a program of research leading to useful 1.06μm AlGaSb avalanche detectors can be evolved. In order of importance the pertinant tasks are:

1) Develop material technology for hole and electron multipliers.
2) Evaluate gain and gain uniformity for both multipliers.
3) Measure F(M) for hole and electron multipliers
4) Evaluate expected rangefinder receiver accuracy.
5) Measure microscopic ionization rates α and β.

The following sections describe our efforts, partly completed to date, toward achieving the goals of this program.

3.2 Materials Growth and Evaluation

1.06μm AlGaSb APD work requires growth of layers with 11.5-15% AlSb (buffer layer), 23-30% AlSb (active layer), and 35-40% AlSb (window layer). Growth procedures for fabricating individual and multiple layer structures of these compositions were devised. n and p-type doping was established as required. Finally, measurements of optical transmission of the active absorbing layer were carried out.

Liquid phase epitaxy was used to fabricate all AlGaSb structures. Semitransparent furnaces were essential in this work. It was found that precise control of the degree of melt supersaturation is necessary in the growth of planar, micron scale AlGaSb epitaxial material. With the transparent furnace, this control could easily be attained through visual observation of the melts. A two-tier, multi-well, graphite boat-slider arrangement with magnetic coupling was used to carry out the growths.

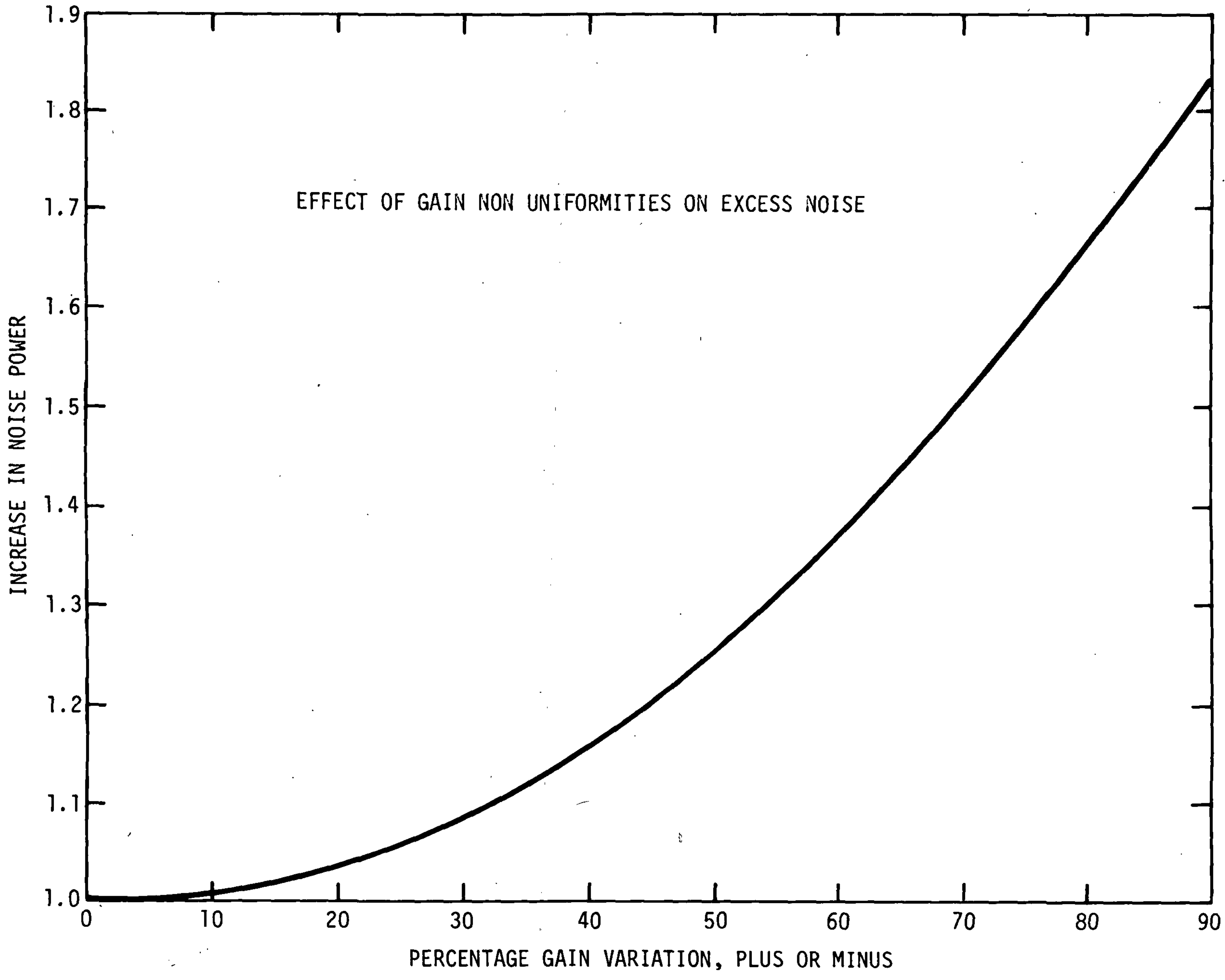

Fig. 3.2 Effect of gain non-uniformities on excess noise.

The starting points for our materials work on this program were the liquidus and soludus phase diagrams shown in Fig. 3.3 and 3.4(1). From these curves, for example, we can determine that, at 500°C, for the active layer of 23% AlSb, we need $X_{Al} \cong 0.01$ and $S_{Sb} = 0.028$ in the liquid. Further refinement of the liquidus data for the three layers (buffer layer, active layer, window layer) was found to be necessary to attain good quality planar structures. The result of this work was a precise temperature and melt composition recipe suitable for fabrication of 4-layer AlGaSb APD structures.

The results are shown in Fig. 3.5 and 3.6 illustrating respectively the as-grown surface and cross-section of a typical growth. The excellent surface morphology and layer planarity are to be noted. Further details of the AlGaSb surface morphology are shown in Fig. 3.7. Growth was accomplished by slow cooling of appropriately supersaturated melts. Typical growth rates of $\gtrsim$ 2μm/min were attained. The high solute concentration (compared with GaAs growth) yields these fairly rapid growth rates.

The minority carrier density and carrier density uniformity of the active n^- layer is one key parameter in AlGaSb APD design. Attainment of $5\times10^{15} - 10^{16}$ average electron density is necessary for low capacitance devices; doping uniformity is clearly of great significance in achieving uniform avalanche gain. Attaining these low electron densities in the GaSb/AlGaSb material system requires careful compensation of the normally p-type material. Growth of GaSb and AlGaSb from Ga rich melts (normal conditions) results in material with a point defect induced background hole density of $\simeq 2\times10^{17}\text{cm}^{-3}$. Thus, in compensated material the average net electron density is

$$n = N_d - 2\times10^{17}$$

and the allowable tolerance in N_d is

$$\left(\frac{\Delta N_d}{N_d}\right) = \left(\frac{\Delta n}{n}\right)\left\{\frac{N_d - 2\times10^{17}}{N_d}\right\} \quad . \tag{3.7}$$

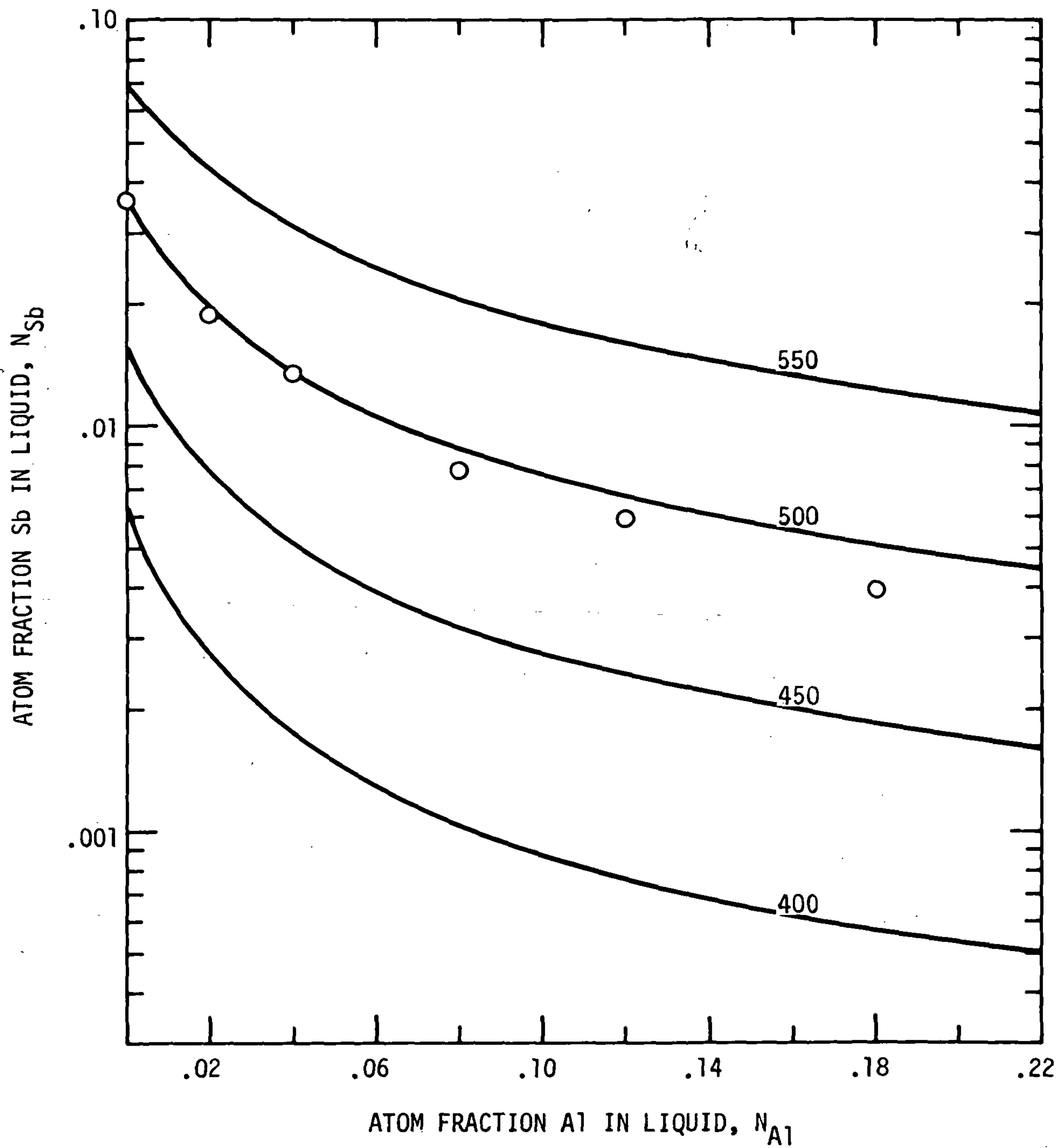

Fig. 3.3 AlGaSb liquidus isotherms

Experimental data points at 500°C and calculated fit using the values of Table 1.

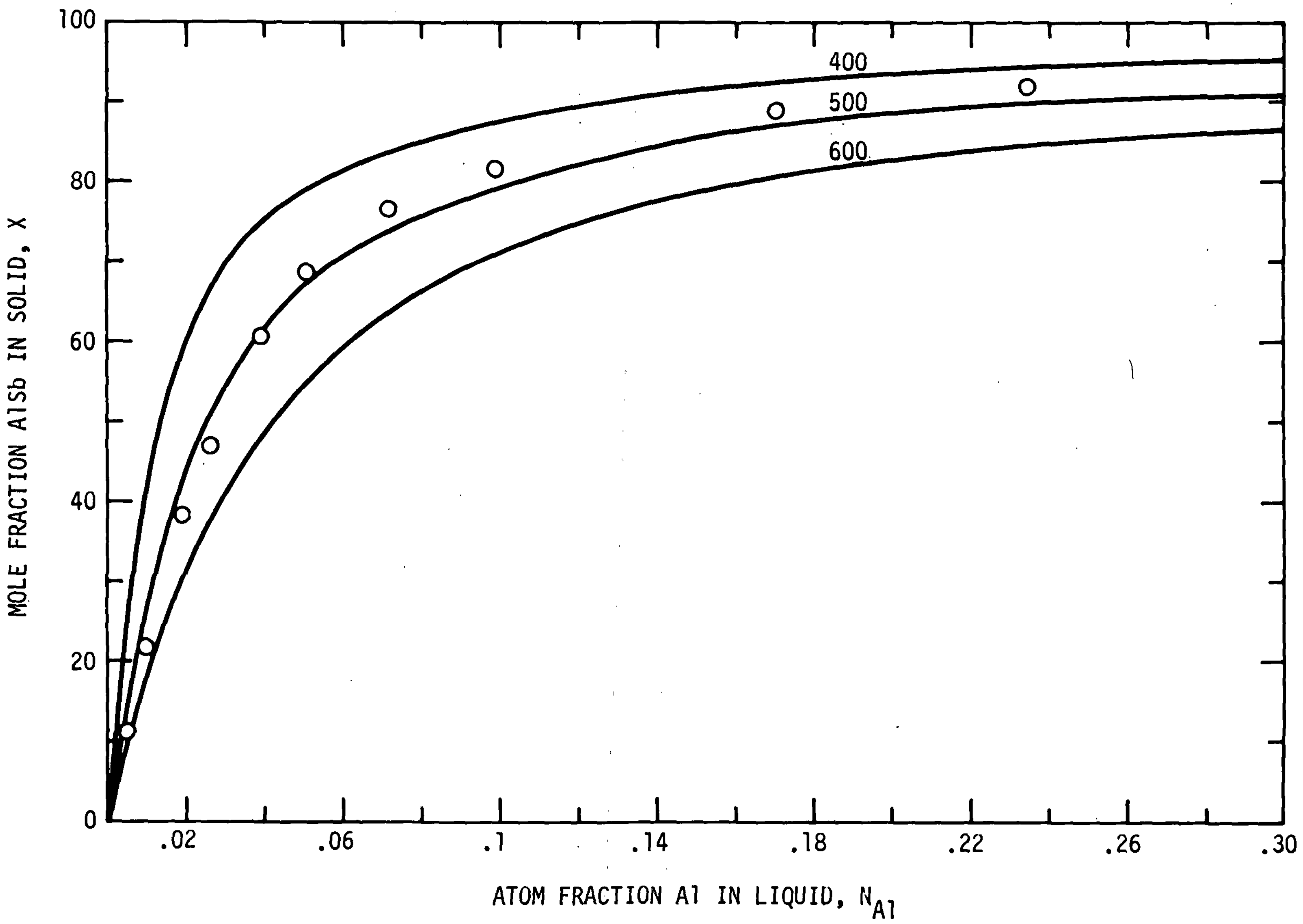

Fig. 3.4 $Al_xGa_{(1-x)}Sb$ Solidus isotherms
Experimental data points at 500°C and computer fit using the values of Table 1.

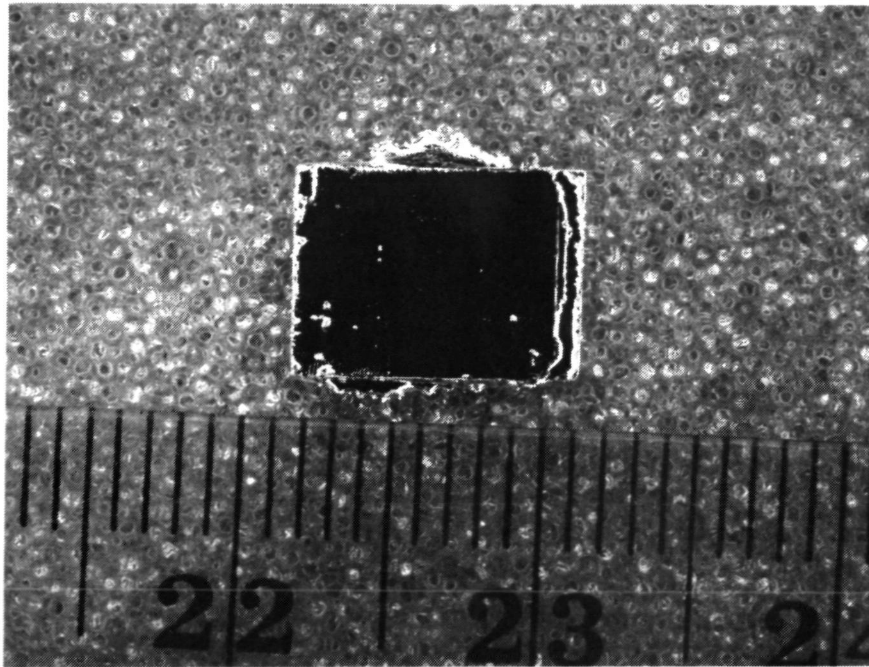

Fig. 3.5 Four layer $Al_xGa_{1-x}Sb$ APD structure. Note excellent growth morphology.

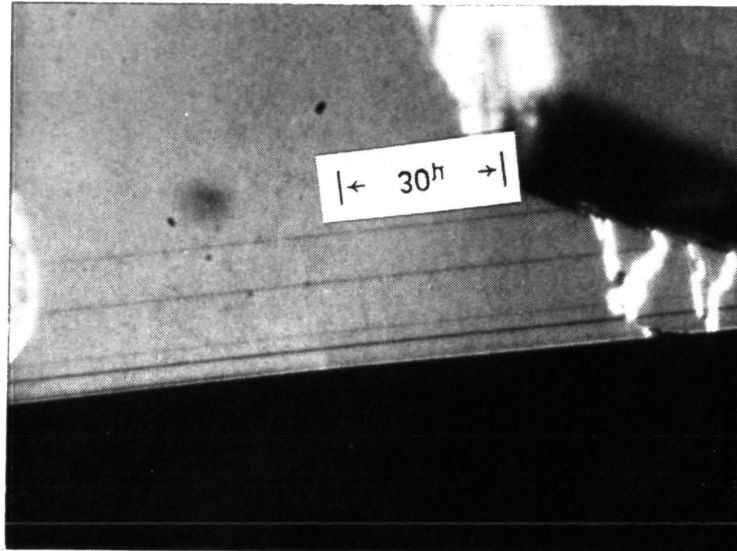

Fig. 3.6 Cleaved cross-section (stained) of four layer 1.06μm $Al_xGa_{1-x}Sb$ APD. Layers grown on n^+ GaSb substrate are: n $Al_{.115}Ga_{.885}Sb/n^-Al_{.23}Ga_{.77}Sb/p^+ Al_{.23}Ga_{.77}Sb/p^+ Al_{.4}Ga_{.6}Sb$.

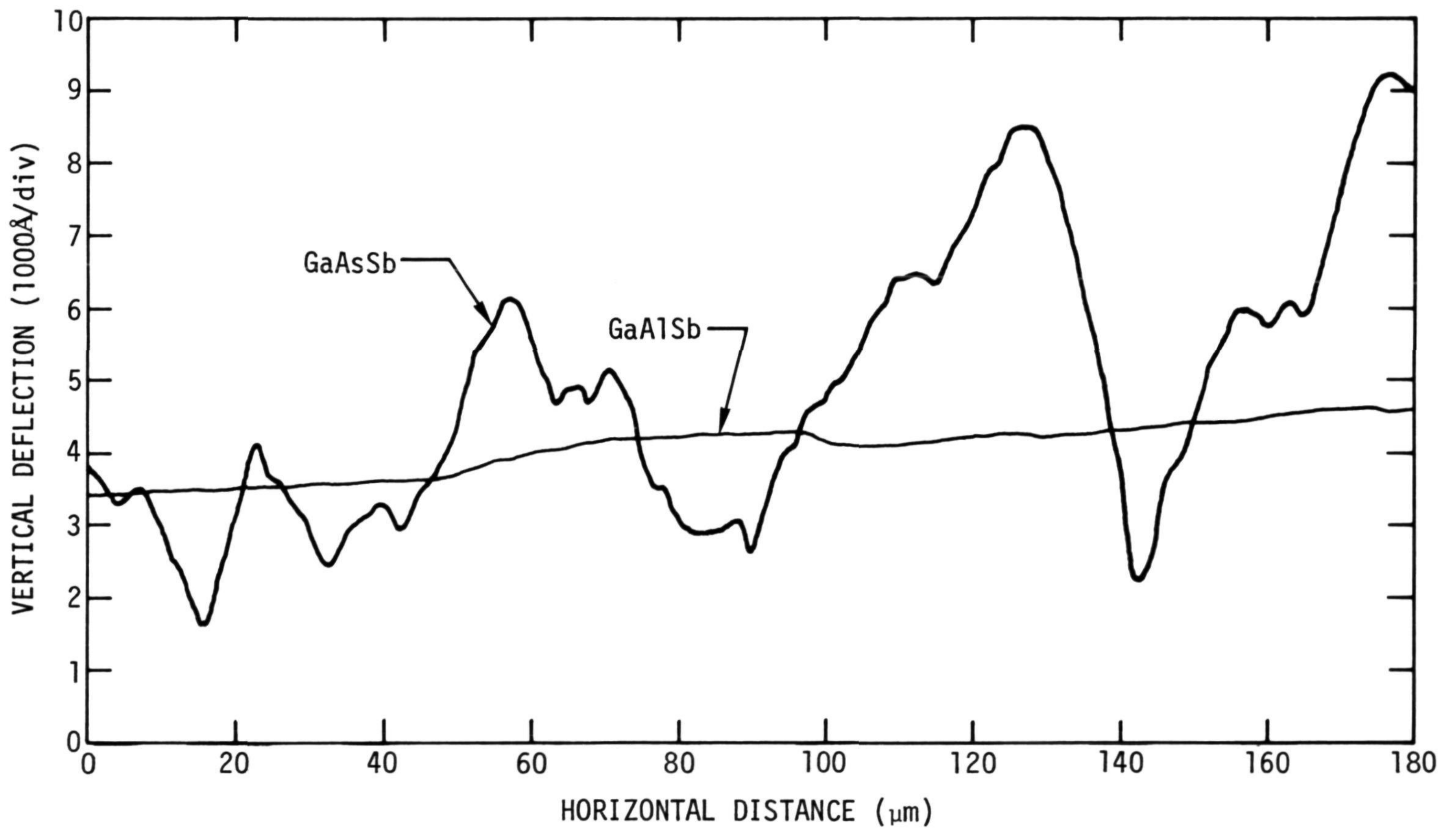

Fig. 3.7 Surface topology of GaAlSb and GaAsSb.

$\frac{\Delta n}{n}$ is the fractional run-to-run variation in electron density.

By extremely careful control, n^- doping densities of 5×10^{16} - $1 \times 10^{16} cm^{-3}$ have been achieved in 23% AlSb material. These are fairly reproducible. The donor used is tellurium, in the form of Te doped GaSb substrate material. The doping profile of a typical low doped n^- layer is shown in Fig. 3.8 (from C-V analysis of p^+n^- junction). The non-uniform profile suggests tellurium depletion as the growth proceeded. Run-to-run doping reproducibility is limited by the accuracy with which the Te can be weighed. From Eq. 3.7, for reproducible ($\Delta n/n \approx 0.2$) growth of 5×10^{15} material, we can tolerate no more than 0.5% fluctuation in N_d. For growth of 23% AlSb layers from appropriate melts, this means that we must weigh out 1 mg ± 5μg of GaSb:Te. For this measurement, a Cahn "Gram" electrobalance was used. On the 0-1 mg scale we have found that this balance can be read to < ± 2μg precision; thus adequate run-to-run reproducibility is available.

Also of great significance is the doping uniformity over the active area of the device. Pertinant numerical calculations are shown in Fig. 3.9. For average avalanche gains of 20-30, we require that the net doping density in the active layer vary by not more than 0.5-1.0% over the active area. Larger fluctuations lead to unacceptable non-uniformities in avalanche gain. Resistivity profiles with micron spatial resolution can be obtained by using photovoltage techniques.

Further, less critical doping measurements were carried out on the buffer layer (11.5% AlSb), termination layer (23% AlSb) and window layer (35% AlSb); other measurements were also carried out on GaSb itself. For the p^+ window layer and termination layer, Ge was used; the distribution coefficient of Ref. 1 gave satisfactory results. Te doped buffer layers with about 2×10^{17} net donor density were used. Studies on these layers and on pure n-type GaSb layers show that considerably more Te must be supplied to the melt to obtain the same doping as the higher AlSb layers. An order of magnitude more Te is required for GaSb than for $Ga_{.77}Al_{.23}Sb$. This is a result of a change in background hole concentration or Te distribution coefficient.

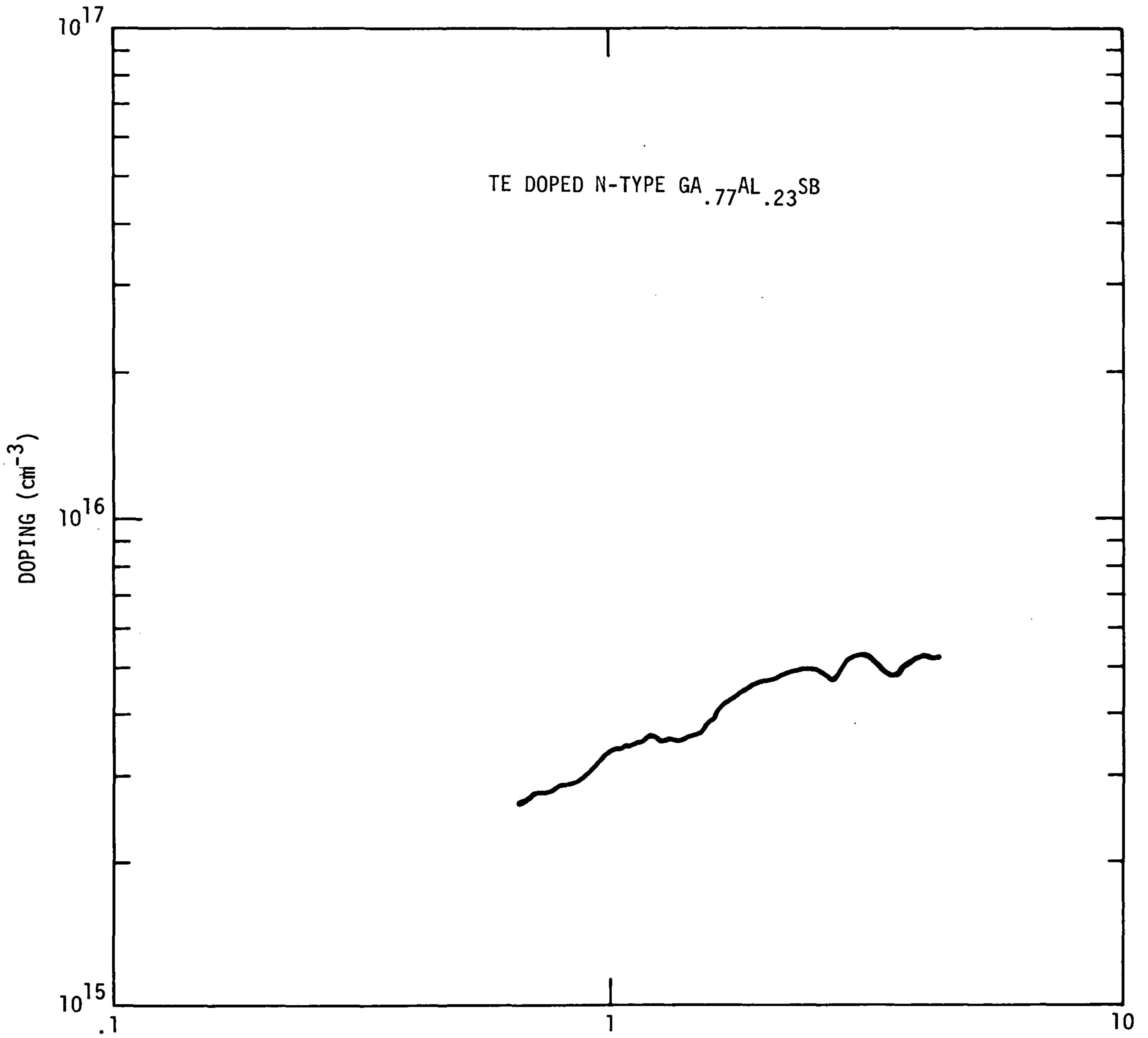

Fig. 3.8 n, Te doped $Ga_{.77}Al_{.23}Sb$.

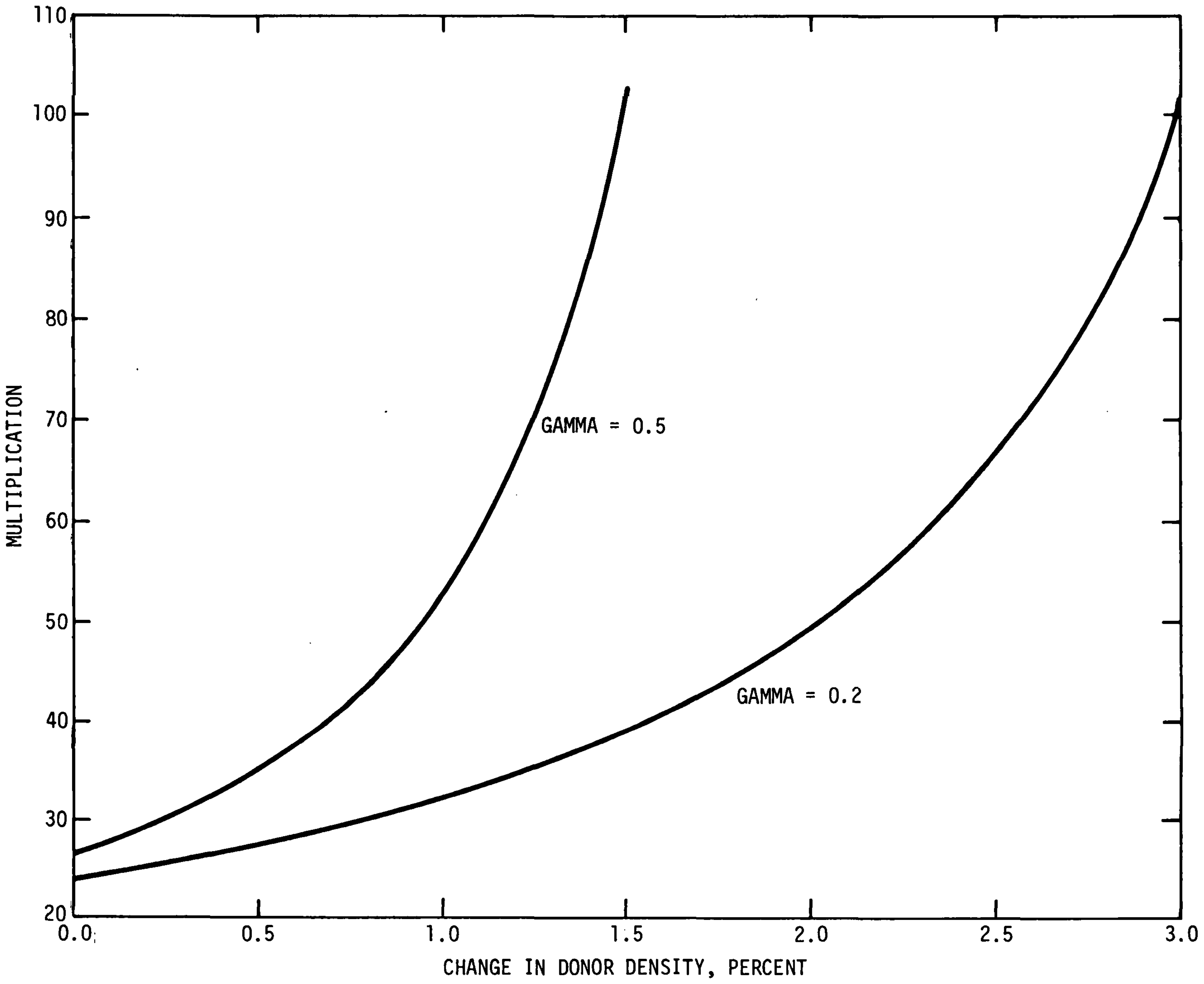

Fig. 3.9 Effect of doping variations on gain. $\gamma = \alpha/\beta$. p^+/n^- junction.

The most important elementary material parameter for photodetector design is the optical absorption, α (not to be confused with the electron ionization rate, also denoted by α). Typically, for most materials systems this parameter is measured routinely, and material composition and depletion region thickness simultaneously adjusted to give the desired quantum efficiency (qe). For a 5μm thick depletion region, and 95% qe, we need $\alpha = 0.6 \times 10^4 cm^{-1}$. Smaller α gives low qe; larger α results in larger dark currents. A serious problem arises when trying to measure the transmission of layers of AlGaSb: the GaSb substrate is opaque at the wavelengths of interest. The same problem arises when measuring the optical transmission of AlGaAs alloys, of great interest for solar cell application.

A new heterojunction device was designed[9] to facilitate optical transmission measurements on these and other alloys; this device is shown in Fig. 3.10. The short circuit photocurrent of the p-n junction gives a direct measure of the optical absorption of the top AlGaSb layer via the relation

$$I_{sc} = I_o{}^{-\alpha(\lambda)t} .$$

While the structure in Fig. 3.10 is in fact relatively easy to grow, and utilizes a simple homojunction p-n junction, time limitations have prevented us from fabricating it and carrying out the measurements.

A simpler, less accurate approach to making the transmission measurements is shown in Fig. 3.11. With this approach (barrier layer omitted), the photocurrent consists of transmission and diffusion components. We have, for large surface recombination velocity (typical of III-V's),

$$\frac{I \text{ diffusion}}{I \text{ transmission}} = \alpha \left[\frac{e^{\alpha\ell-\ell}-1}{\alpha - 1} - \frac{e^{-\ell+\alpha\ell} - e^{-2\ell}}{\alpha + 1} \right]$$

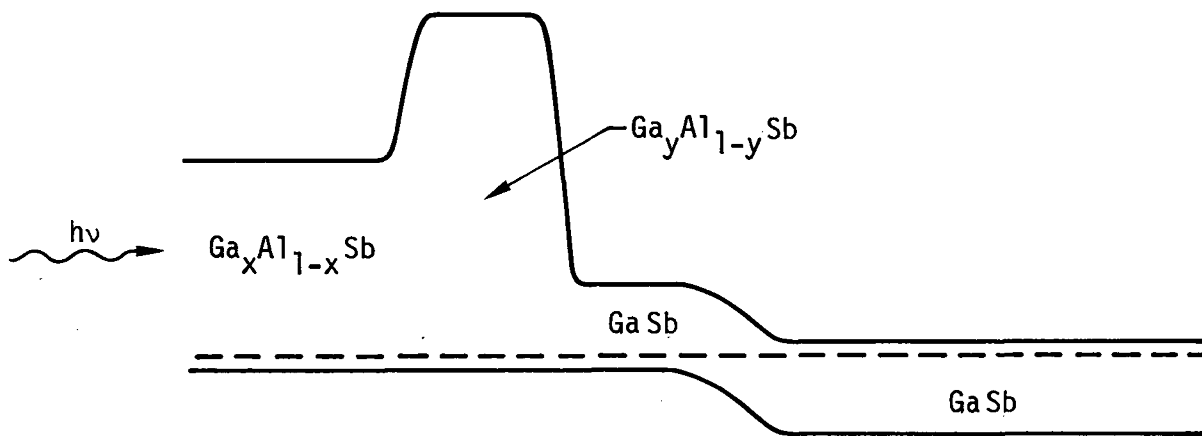

Fig. 3.10 Heterojunction device structure for optical transmission measurements. The photocurrent measured in the GaSb p-n junction is due solely to light transmitted through the top $Ga_{1-x}Al_xSb$ layer.

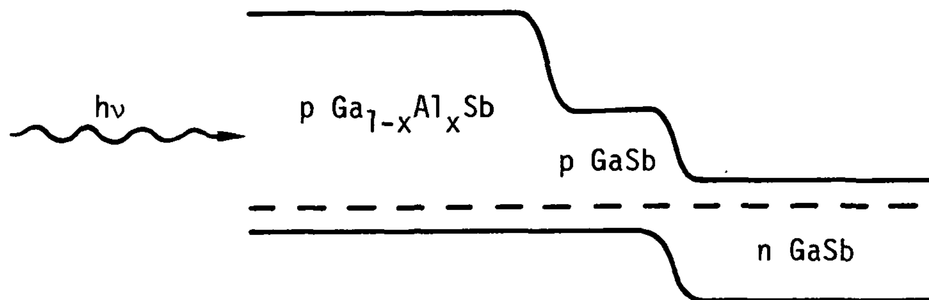

Fig. 3.11 p-n junction structure for optical transmission measurement.

where L = minority carrier diffusion length.

α = optical absorption coefficient, in units of 1/L

ℓ = layer thickness, units of 1/L

From study of this equation we see that (for layer thickness at least 2 or 3 diffusion lengths) the diffusion component is small as long as $\alpha < 1/L$. Thus, usable direct gap measurements can be made in material with small diffusion length.

3.3 Device Processing

For high speed receiver applications small area mesa diodes have to be fabricated and packaged in 50Ω-microwave mounts or hybrid integrated with a low noise preamplifier. This poses some special, but not insurmountable, problems for AlGaSb detectors. For these devices, light must be brought in through the mesa side and consideration needs to be given to fabricating a diode with a small junction diameter but adequate optical area.

The diode structure fabricated under the current program is shown in Fig. 3.12. Contacts are evaporated, and then 3 mil x 3 mil mesas are chemically etched. Mesa contact is 1 mil diameter. These diodes have been useful for test purposes, but the 1 mil mesa metalization is too small for wire bonding.

A new set of masks to solve this problem has been designed and fabricated. The resulting mesa diodes are shaped into "figure eights" with one pad for wire bonding and one pad for optical reception. The specifications for these test diodes, and a "standard" GaAsSb 3 mil diameter mesa diode are shown in Table 3.1. All the diodes in this table can be bonded; the AlGaSb devices differ in optical and/or electrical areas. This table shows that practical AlGaSb device structures can be designed. The electrical area required for bonding is small but, unfortunately, not zero. Note also that the diode capacitance in practice is in parallel with the preamp input capacitance. For receivers suitable for low noise 2 cm rangefinding this latter capacitance is about 0.28pF.

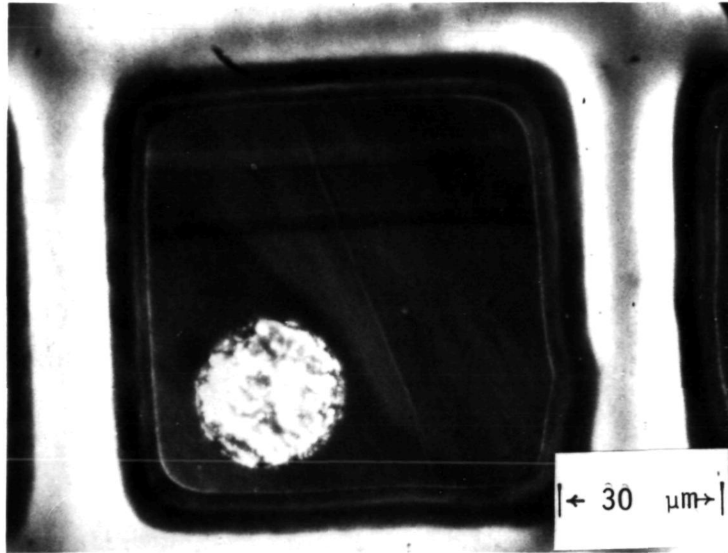

Fig. 3.12 Etched mesa -- 3 mil x 3 mil with 1 mil metallization pad.

	Optical diameter	Calculated Capacitance (W=4μm)
GaAsSb	3 mil	0.14 pf
AlGaSb I	2 mil	0.13 pf
AlGaSb II	2 mil	0.17 pf
AlGaSb III	3.1 mil	0.26 pf
AlGaSb IV	2.5 mil	0.17 pf

Table 3.1 Specifications for new AlGaSb devices.

Achieving the high quantum efficiency available requires a suitable antireflection coating. The optical dielectric constant of $Al_{.23}Ga_{.77}Sb$ is 11.21 (n = 3.35). Sputtered films of Si_3N_4 (n = 2.0) are easily prepared and give a good index match to air. A 1325Å thick Si_3N_4 film on $Al_{23}Ga_{77}Sb$ will have 0.8% reflectivity at 1.06μm. This should be adequate.

3.4 Device Performance

Three and four layer AlGaSb APD's were fabricated as outlined above. Measurements of I-V, C-V, photoresponse and avalanche multiplication were made. Preliminary work on multiplication noise was also carried out. The three layer AlGaSb structure fabricated is shown in Fig. 3.13. The four layer devices were similar, with the addition of a transparent p^+ $Al_{35}Ga_{65}Sb$ layer. These structures, with the layer sequence shown in Fig. 3.13 are ideal for multiplication measurements. Practical diodes would probably use the opposite sequence of layers as illustrated in Fig. 3.2. All multiplication measurements made were <u>electron</u> multiplication; time did not permit investigation of hole multipliers.

The capacitance-voltage characteristic of our best reproducible device is shown in Fig. 3.14. Capacitance near breakdown for this 3 mil x 3 mil device is less than 0.18pF. For a 3 mil diameter circuiar mesa this material would give a capacitance of 0.147 pF. Our best 3 mil GaAsSb diodes have junction capacitance of 0.11 pF[10]. Thus, the AlGaSb devices are good, but not yet equivalent to the best GaAsSb results.

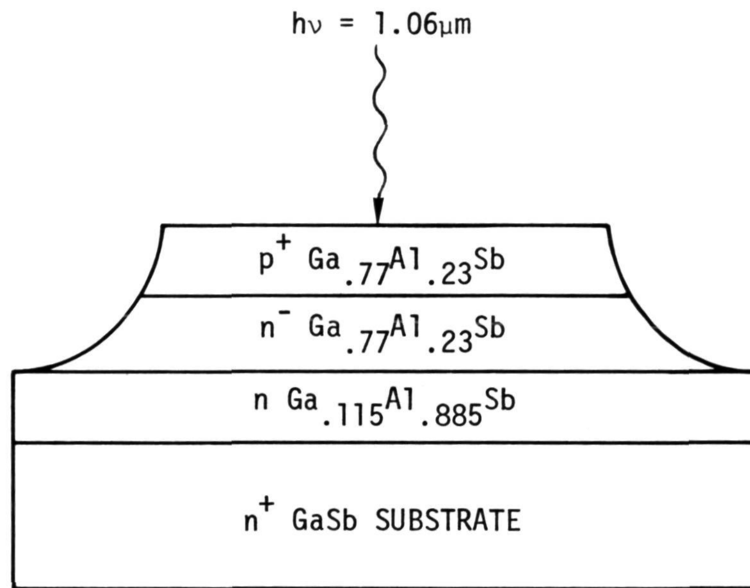

Fig. 3.13 $Al_xGa_{1-x}Sb$ APD structure.

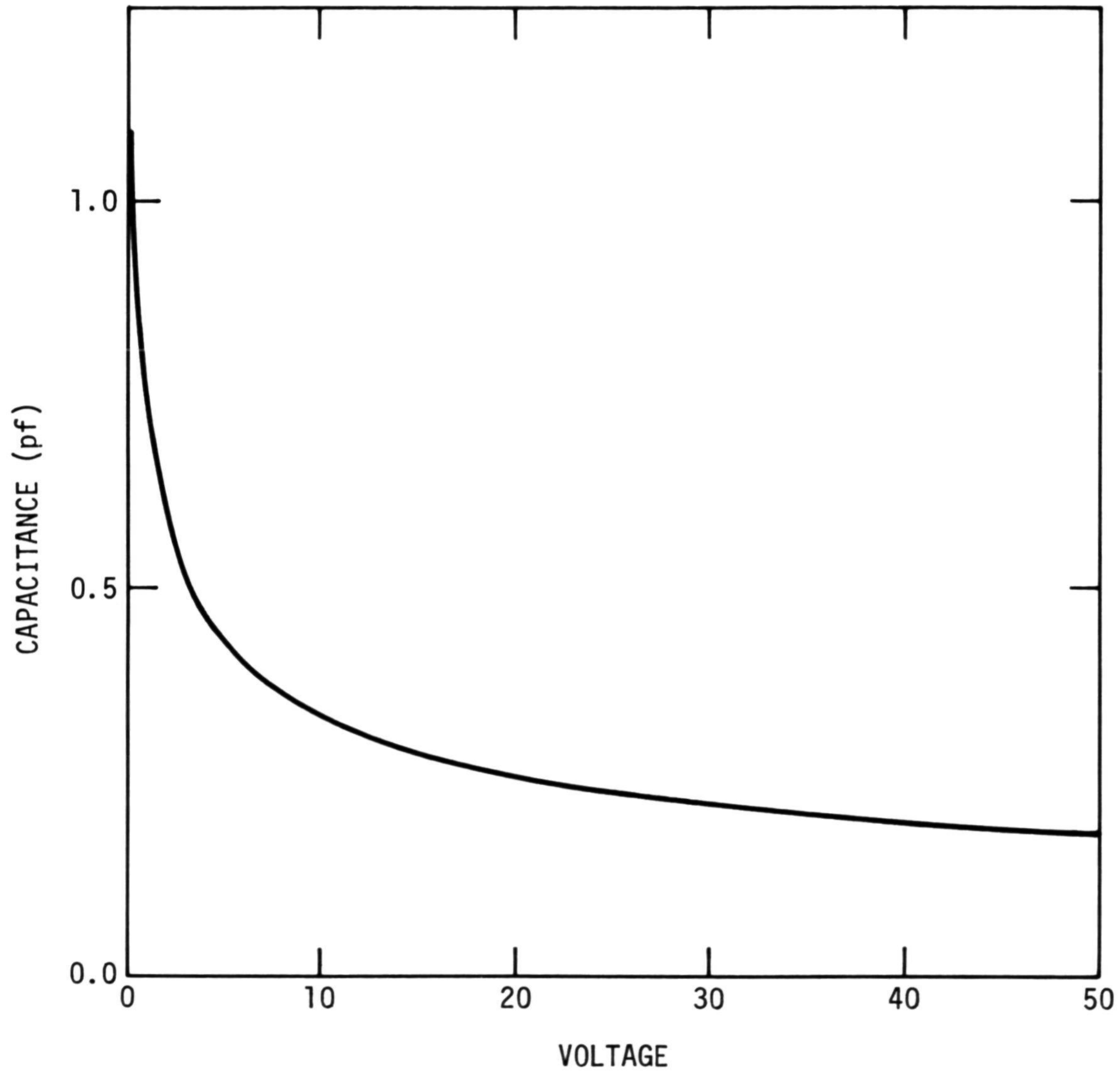

Fig. 3.14 C-V for 3 mil x 3 mil AlGaSb APD.

The relative quantum efficiency of three-layer and four layer AlGaSb APD structures is shown in Fig. 3.15 and 3.16, respectively. These results are obtained using the Cary-14 monochrometer with a feedback circuit to maintain constant light intensity. The long wavelength cut-on is similar in both devices and is determined by the bandgap of the $Al_{.23}Ga_{.77}Sb$. The short wave response of the 4 layer structure is enhanced by the transparent window. Absolute quantum efficiency (corrected for reflection loss) of this device at 1.064μm was measured to be 60%.

Avalanche gain measurements are carried out with our laser scanning microscope. The 1.064 m Nd:YAG beam is focused with a 0.5 na, 40X, 1.7cm reflective objective. The long working distance lens allows measurements to be made on probe contacted (i.e. unpackaged) devices. The focused beam is scanned across the device active area using moving coil mirrors. In this fashion area displays of avalanche gain with spatial resolution of 2-3μm (limited by lateral diffusion of carriers) can be obtained.

Avalanche gain and leakage current for a typical good device (F10-8/31/76) are shown in Fig. 3.17. Device is a 3 mil x 3 mil mesa. These measurements were made with the laser beam chopped at 1600 Hz. The multiplication is that representative of the area averaged gain; maximum average gain is about 10. Leakage current near breakdown is less than 1μa. Other material with good reverse leakage and higher breakdown was fabricated. A I-V characteristic of a good "high voltage" diode is shown in Fig. 3.18. Diodes with breakdown of 110V have been fabricated, but these showed ~ 6μa reverse leakage current near breakdown.

Measurements were made of the pulse response of the AlGaSb avalanche photodiodes. These were carried out with the Q-switched Nd:YAG laser. Since our devices were unpackaged, measurements with mode-locked signal were not considered. The APD pulse response with the without gain (low and high bias) is shown in Fig. 3.19. Avalanche gain here is about 17. For these measurements, the beam was focused near a high gain region; thus the area average gain on this device was somewhat lower.

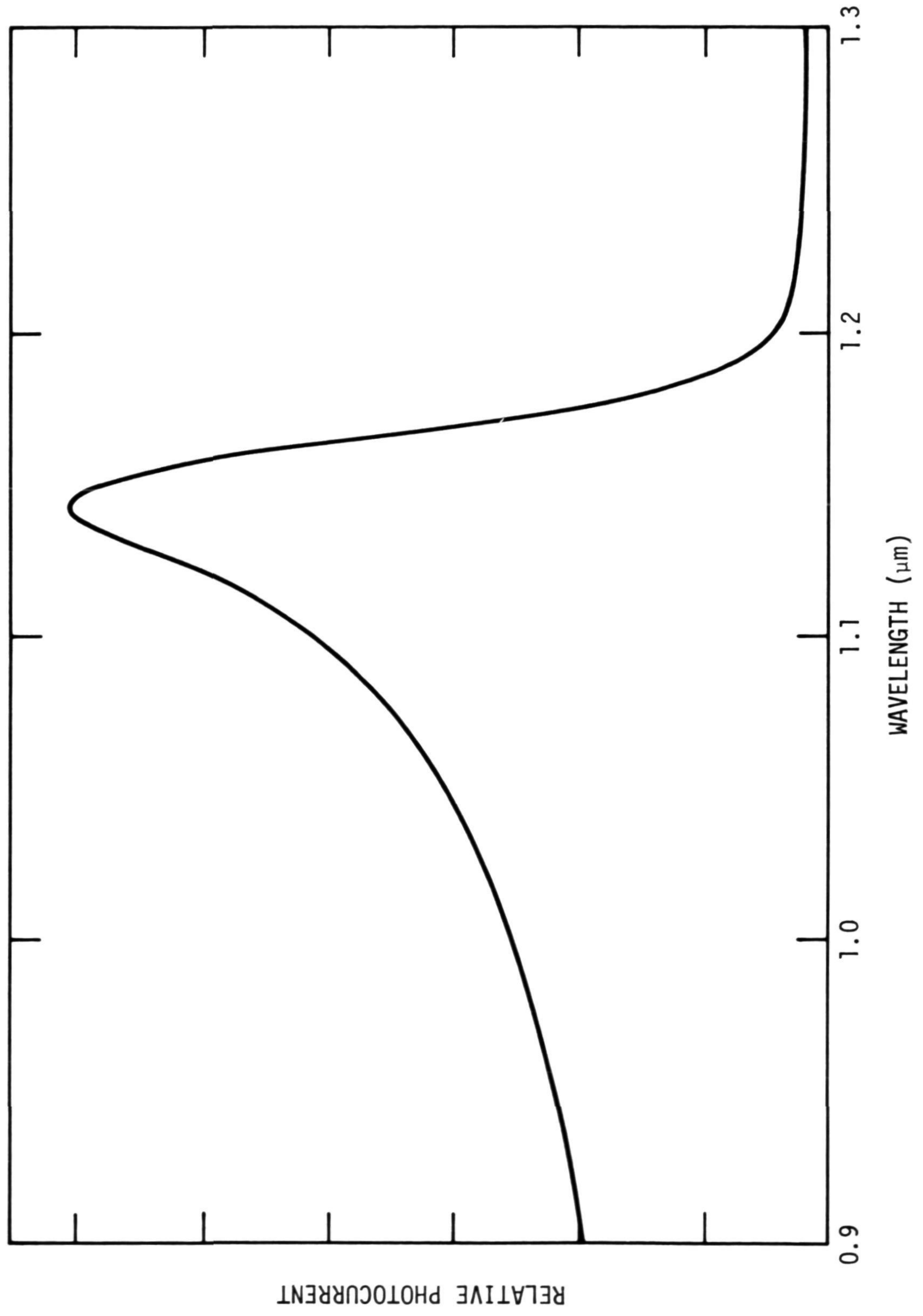

Fig. 3.15 Photoresponse of 3 layer AlGaSb APD.

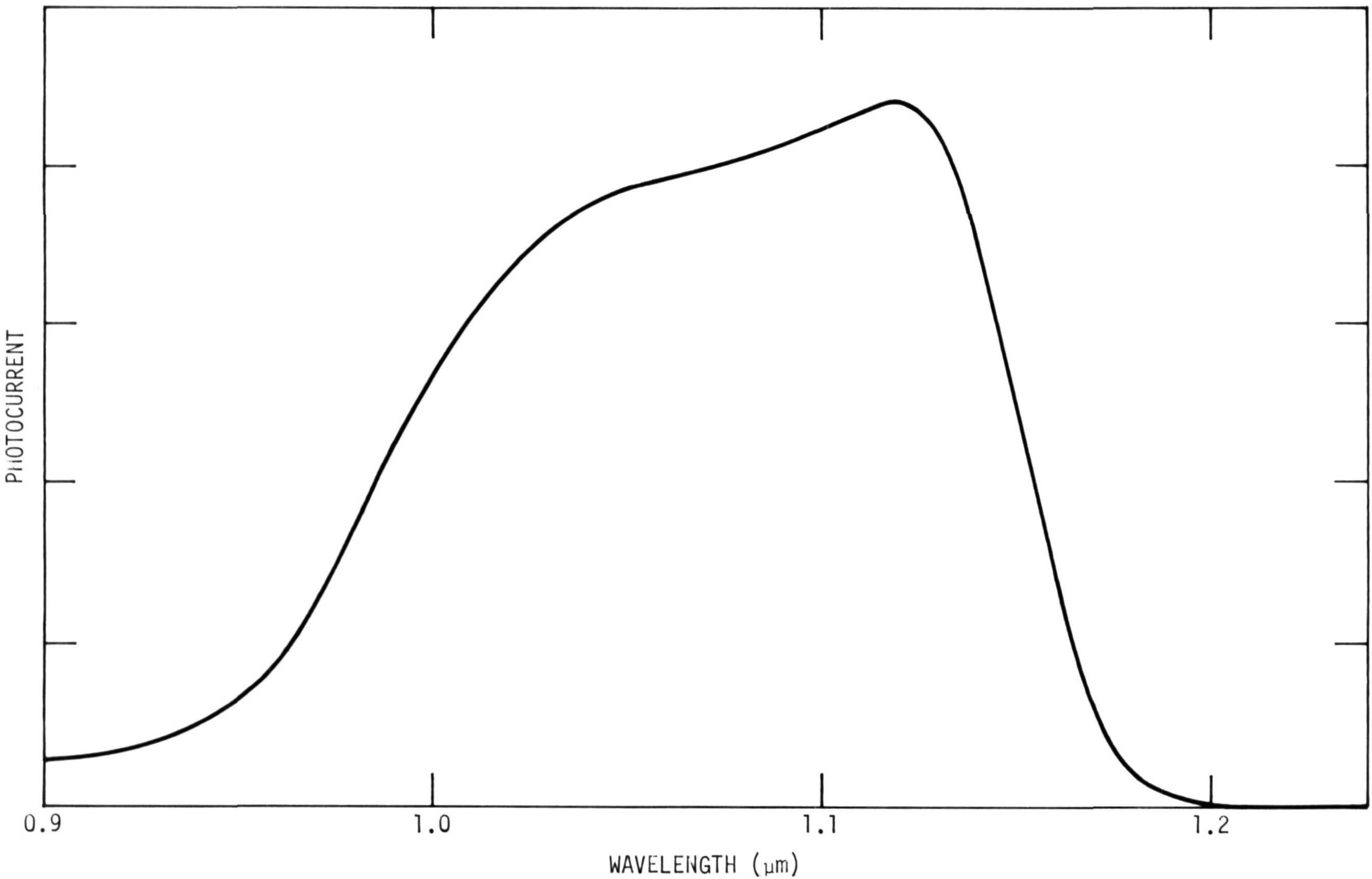

Fig. 3.16 Photoresponse of 4 layer AlGaSb APD.

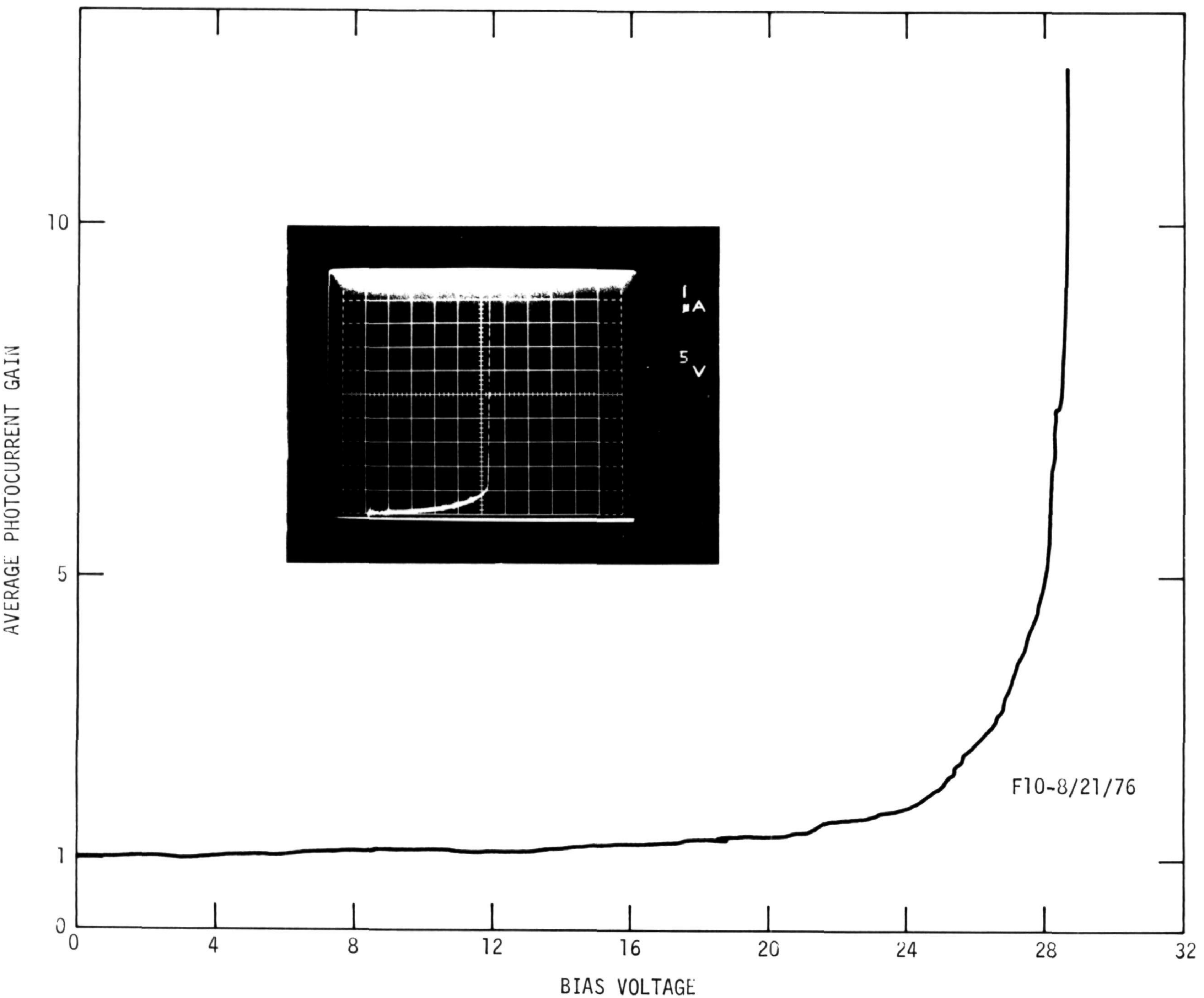

Fig. 3.17 Reverse bias I-V characteristic and photocurrent gain for a 1.064μm $Al_{.23}Ga_{.77}Sb$ avalanche photodiode.

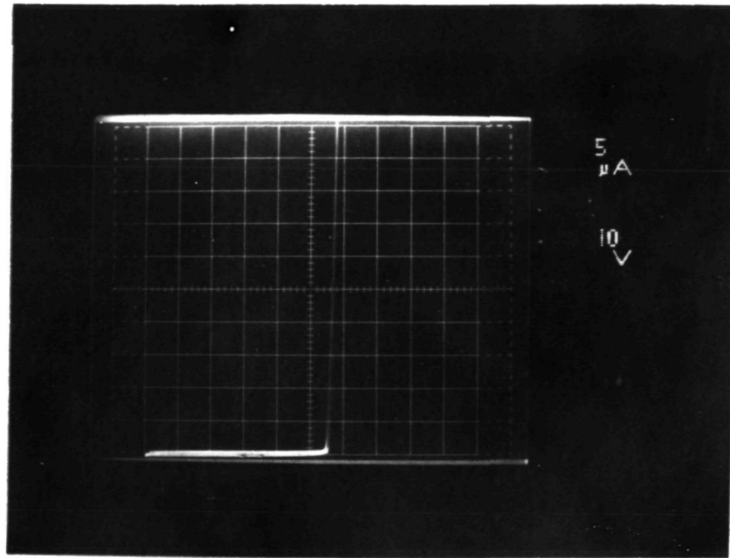

Fig. 3.18 High breakdown AlGaSb photodiode; growth F10-9/23/76.

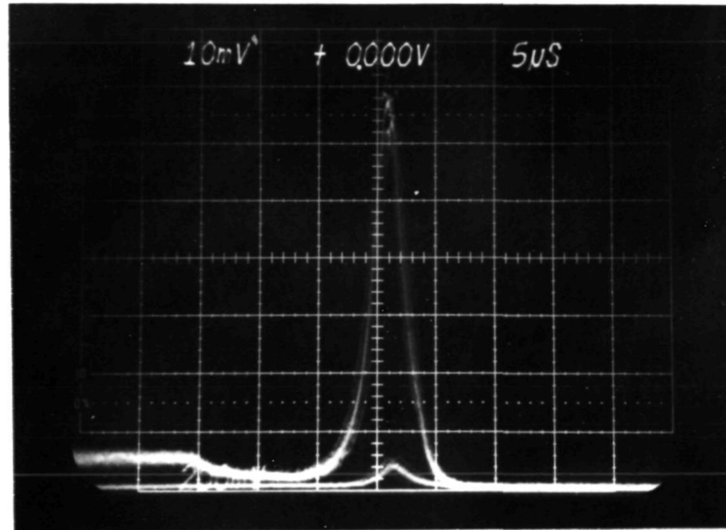

Fig. 3.19 APD pulse response. Diode from growth F9-4/23/76.

All avalanche photodiodes show some gain non-uniformities. These gain non-uniformities can increase the excess multiplication noise, and of course cause drift in the return signal amplitude. The latter is less serious for rangefinder applications than for digital communication systems.

Linear scans through four separate devices from growths F10-5/24/76 and F10-8/31/76, Fig. 3.20 and 3.21, indicate the present state-of-the-art in AlGaSb detectors. These detectors are characterized by the broad scale non-uniformities shown. Doping fluctuations or compositional variations could be responsible for these gain non-uniformities.

Avalanche multiplication noise measurements were not completed during the course of this contract; however effort was spent on design and construction of a suitable instrumentation system. This is discussed here.

The quantity of interest is the excess noise factor F(M); the experimentally observable quantity is the mean square photodiode noise current in bandwidth Δf:

$$\langle i^2 \rangle = 2qM^2F(M)\eta I_{ph}\Delta f + \left(2qI_{dark} + \frac{4kT}{R_f} + S_{stray}\right)\Delta f.$$

I_{ph} = incident photon current.

η = detector quantum efficiency.

I_{dark} = detector dark current.

R_f = transimpedance.

S_{stray} = spectral density of pick-up noise.

Accurate noise measurements then require that the unmultiplied photocurrent shot-noise clearly dominate the noise due to detector surface leakage, the receiver input noise, and the pickup noise. To ensure this condition a wide dynamic range, wide bandwidth transimpedance amplifier was designed and constructed. This unit has an order of magnitude better dynamic range than our commercially available current amplifier (Keithley 427). A filtered tungsten ribbon filament lamp is a suitable low-noise light source for these measurements[11]. This source has a maximum brightness (200Å filter) of about

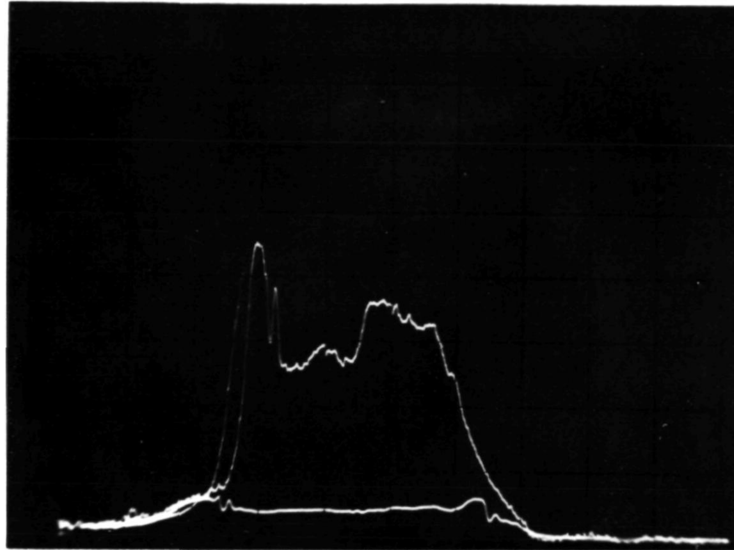

(a)

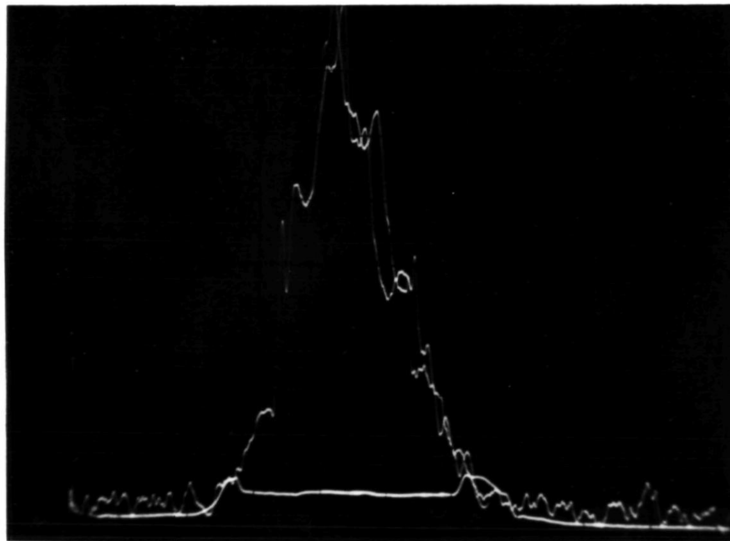

(b)

Fig. 3.20 Linear scans showing gain in 3 mil dia. mesa devices from growth F10-5/24/76.(a) $\overline{M}$ = 8.5; (b) $\overline{M}$ = 12.

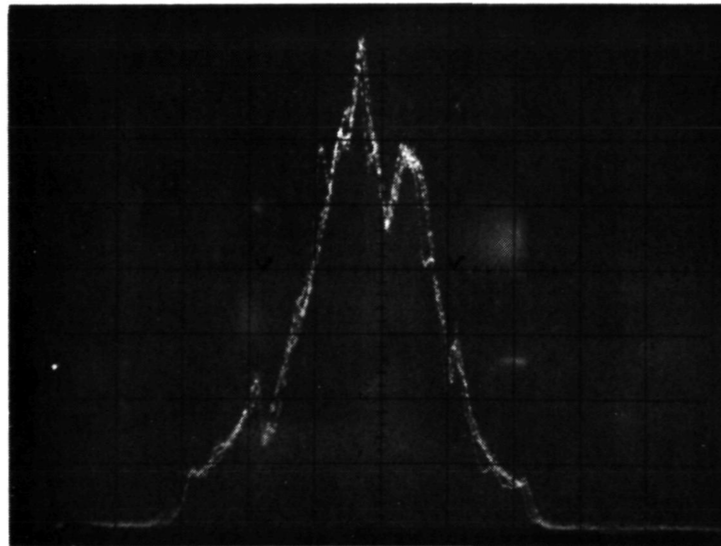

(a)

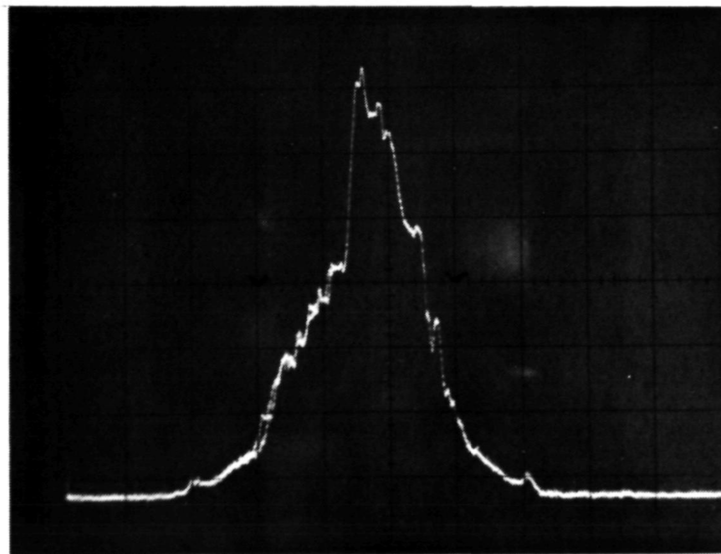

(b)

Fig. 3.21 Gain profiles from growth F10-8/21/76. 3 mil x 3 mil square mesa devices. (a) $\overline{M}$ = 10; (b) $\overline{M}$ = 17.5

0.91 $\frac{\text{watts}}{\text{cm}^2\text{-str.}}$ and can provide 3.6μw of optical power in a 1 mil diameter focus (0.5 numerical aperture). This flux density is enough to dominate the photodiode dark current, reciever thermal noise, and with suitable packaging, the stray noise. Note than an appropriately tuned high-brightness LED might be a considerably better source for these noise measurements. These diodes have brightnesses of >50 watts/cm^2-str., and will become available to us through our Air Force contract work.

4.0 CONCLUSIONS AND RECOMMENDATIONS

The major conclusion of this work is that useful 1.06μm avalanche photodiodes can be fabricated from AlGaSb ternary alloys. Under the current program we have developed diodes with average gains of 10, dark currents less than 1μa, and junction capacitance less than 0.2 pf. At the start of this work, no p-n junction diodes of $Al_{.23}Ga_{.77}Sb$ had been fabricated by anyone. We developed the material and device processing technologies to support these accomplishments. The work performed under this contract provides a promising foundation for fabrication of the 1.06μm rangefinder receivers.

Efforts now need to be focussed on (1) hole multipliers, (2) gain uniformity, (3) excess noise factor, and (4) systems modelling. There is reason to believe that the band structure of $Al_{.23}Ga_{.77}Sb$ favors hole multiplication ($\beta < \alpha$). Thus, structures complementary to those fabricated under this program need to be tested. Work needs to be aimed at practical diodes that can be packaged into high-speed mounts (or receivers). These diodes must then be completely characterized: gain, gain uniformity, excess noise quantum efficiency, and risetime are the key parameters. These data can then be utilized in suitable simulations to determine the expected accuracy of avalanche detector-based receiver. We strongly recommend that these tasks be undertaken. The results of the current program suggest a high probability that they will lead to APDs suitable for precision 1.06μm rangefinding.

5.0 REFERENCES

1. S. J. Anderson, F. W. Scholl, J. S. Harris, "AlGaSb Alloys for 1-1.8μm Heterojunction Devices," 1976 GaAs Conference, St. Louis, Mo.

2. P. P. Webb, R. J. McIntyre, J. Conradi, RCA Review, 35, 234 (1974).

3. C. A. Lee, R. A. Logan, R. L. Batdorf, J. J. Kleinack, W. Wiegmann, Phys. Rev., A134, 761 (1964).

4. D. McCarthy, Ph.D. Thesis, Cornell University, June 1974.

5. G. E. Stillman, C. M. Wolfe, A. G. Foyt, W. T. Lindley, Appl. Phys. Lett., 24, 8 (1974).

6. W. T. Lindley, R. J. Phelan, C. M. Wolfe, A. G. Foyt, Appl. Phys. Lett., 14, 197 (1969).

7. T. P. Pearsall, R. Nahory, M. A. Pollack, Appl. Phys. Lett., 27, 330 (1975).

8. G. E. Stillman, C. M. Wolfe, J. A. Rossi, A. G. Foyt, Appl. Phys. Lett., 24, 471 (1974).

9. Rockwell Science Center IR&D, 1976, Project No. 843.

10. R. C. Eden, Final Report for NASA Contract No. NAS5-23134, Dec. 1975.

11. R. C. Eden, private communication.